Hot and dense lattice QCD in the strong coupling limit

Yusuke Nishida

January 7, 2004

Abstract

Quantum chromodynamics (QCD) with colors $N_{\rm c}$ and flavors $N_{\rm f}$ at finite temperature (T), baryon chemical potential ($\mu_{\rm B}$) and isospin chemical potential ($\mu_{\rm I}$) is studied in the strong coupling limit on the lattice with staggered fermions. With the use of the large dimensional expansion and the mean field approximation, we derive an effective action written in terms of the chiral condensate and the diquark/pion condensate as a function of T, $\mu_{\rm B}$ and $\mu_{\rm I}$. Firstly, we clarify the phase structure for $N_{\rm c} = 2$, $N_{\rm f} = 4$ with special emphasis on the interplay among the chiral condensate, the diquark condensate and the baryon density in the T-$\mu_{\rm B}$-m space. Simple analytical formulae are also derived without assuming $\mu_{\rm B}$ nor m being small. Then the phase structure in the space of T and $\mu_{\rm B}$ is elucidated for $N_{\rm c} \geq 3$ and $N_{\rm f} = 4, 8$, and simple analytical formulae for critical line of chiral phase transition and tricritical point are derived. Effects of finite quark mass (m) and finite $\mu_{\rm I}$ on the phase diagram are discussed. We also investigate the phase structure for $N_{\rm c} \geq 3$, $N_{\rm f} = 8$ in the space of T, $\mu_{\rm I}$ and m, and clarify a correspondence between the color SU(3) QCD with finite isospin density and the color SU(2) QCD with finite baryon density. Comparisons of our results to those from recent Monte-Carlo lattice simulations in finite density QCD are given.

Master Thesis

Department of Physics, University of Tokyo

Contents

1 Introduction

To reveal the nature of matter under extreme conditions in Quantum Chromodynamics (QCD) is one of the most interesting and challenging problems in hadron physics. At present the Relativistic Heavy Ion Collider (RHIC) experiments at Brookhaven National Laboratory are running in order to create a new state of hot matter, the quark gluon plasma [1, 2]. On the other hand, there have been proposed various novel states of dense matter at low temperature which are relevant to the physics of neutron star interiors, such as the $^3P_2$ neutron superfluidity [3], the pion [4] and kaon [5] condensations and so on. Furthermore, if the baryon density reaches as much as the tenth of nuclear density at the core of the neutron stars, quark matter in color-superconducting state may be realized [6].

One of the first principle methods to solve QCD is the numerical simulation on the basis of the Monte-Carlo method. This has been successfully applied to study the chiral and deconfinement phase transitions at finite temperature ($T \neq 0$) with zero baryon chemical potential ($\mu_{\rm B} = 0$) [7]. On the other hand, the lattice QCD simulation has an intrinsic difficulty at finite $\mu_{\rm B}$ due to the complex fermion determinant. Recently new approaches have been proposed to attack the problem in $\mathrm{SU_c}(3)$ QCD at finite $\mu_{\rm B}$ [8], such as the improved reweighting method [9], the Taylor expansion method around $\mu_{\rm B} = 0$ [10] and the analytical continuation from imaginary $\mu_{\rm B}$ [11, 12]. They have indeed given us some idea about the phase structure of QCD, e.g. the existence of the critical endpoint of chiral phase transition and the determination of the slope on the critical line. They are, however, inevitably restricted either to the simulations on a small lattice volume or to the low $\mu_{\rm B}$ region near the critical line. Alternative attempts have been also made to study theories with positive fermion determinant, which include color $\mathrm{SU_c}(2)$ QCD with finite $\mu_{\rm B}$ [13, 14] and color $\mathrm{SU_c}(3)$ QCD with finite isospin chemical potential ($\mu_{\rm I}$) [15, 16].

In this thesis we consider the strong coupling limit of $\mathrm{SU_c}(2)$ [17, 18, 19] and $\mathrm{SU_c}(3)$ lattice QCD [20, 21, 22, 23, 24, 25] and make an extensive study of its phase structure with the use of the effective potential analytically calculated at finite T, $\mu_{\rm B}$, $\mu_{\rm I}$ and the quark mass m. The phases obtained as functions of these variables are not easily accessible in Monte-Carlo simulations and thus give us some insights into hot and dense QCD. Note that our approach has closer connection to QCD than other complementary approaches based on the Nambu−Jona-Lasinio model [26], the random matrix model [27] and the Schwinger-Dyson method [28, 29].

This thesis is organized as follows: Sec. 2 is devoted to the formulation of strong coupling lattice QCD. We explain how to derive an effective free energy starting from the lattice action in the strong coupling limit with one species of staggered fermion (corresponding to $N_{\rm f} = 4$ flavors in the continuum limit) by the use of the large dimensional expansion.

In Sec. 3, discussion on the Pauli-Gürsey symmetry of $\mathrm{SU_c}(2)$ QCD is firstly given at Sec. 3.1. Then we derive an effective free energy $F_{\rm eff}[\sigma, \Delta]$ with $N_{\rm c} = 2$ and $N_{\rm f} = 4$ by introducing the auxiliary fields σ and Δ corresponding to the chiral and diquark condensates and employing the mean field approximation (Sec. 3.2). The resultant free energy is enough simple so that one can make analytical studies in the chiral limit $m = 0$ with finite T and $\mu_{\rm B}$, and in the zero temperature limit $T = 0$ with finite $\mu_{\rm B}$ and m. Sec. 3.3 is devoted to such studies and useful relations of the critical temperature and chemical potential are derived. In Sec. 3.4, we make numerical analyses on the chiral and diquark condensates as well as the quark number density as functions of T, $\mu_{\rm B}$, and m. The phase structure of $\mathrm{SU_c}(2)$ QCD at strong coupling is clarified in the three dimensional T-$\mu_{\rm B}$-m space.

In Sec. 4, we consider color $\mathrm{SU}(N_{\rm c} \geq 3)$ QCD with finite temperature and baryon density. Firstly, we derive an effective free energy in terms of a scalar mode σ and a pseudoscalar mode π for $N_{\rm f} = 4$ (Sec. 4.1). The resultant free energy is simple enough so that one can make analytical studies at least in the chiral limit $m = 0$ with finite T and $\mu_{\rm B}$. Sec. 4.2 is devoted to such studies and useful formulae of the critical temperature and critical chemical potential for the chiral restoration are derived. Especially we can present an analytical expression for the temperature and baryon chemical potential of the tricritical point. In Sec. 4.3, we analyze the chiral condensate and baryon density as functions of $\mu_{\rm B}$

and show the phase diagram in the plane of T and $\mu_{\rm B}$ for $N_{\rm c} = 3, N_{\rm f} = 4$. We discuss the effect of finite quark mass m on the phase diagram of QCD and comparison to the results from recent lattice simulations are given here.

In Sec. 5, we consider the strong coupling lattice QCD with isospin chemical potential as well as T and $\mu_{\rm B}$. In order to include $\mu_{\rm I}$, we extend the formulation studied in Sec. 2 to with two species of staggered fermion, which corresponds to $N_{\rm f} = 8$ flavor QCD in the continuum limit (Sec. 5.1). Then we restrict ourselves to two particular cases: One is at finite T, finite $\mu_{\rm B}$ and *small* $\mu_{\rm I}$ (Sec. 5.2). The other is at finite T, finite $\mu_{\rm I}$ and *zero* $\mu_{\rm B}$ (Sec. 5.3). For each case, we derive and analyze an analytical expression for the effective free energy and show the phase diagram in terms of T and $\mu_{\rm B}$ or $\mu_{\rm I}$ for $N_{\rm c} = 3, N_{\rm f} = 8$. In Sec. 5.2, we discuss the effect of increasing $N_{\rm f}$ and that of finite $\mu_{\rm I}$ on the phase diagram of QCD in T-$\mu_{\rm B}$ plane. In Sec. 5.3, comparison to the results from lattice simulations and discussion on a correspondence between QCD with finite $\mu_{\rm I}$ and $\mathrm{SU_c}(2)$ QCD with finite $\mu_{\rm B}$ are given.

Summary and discussion are given in Sec. 6. In Appendices A, B and C, we give some technical details in deriving the effective free energy. Note that Sec. 3 in this thesis is based on a recent paper by the author [30] and Sec. 4, 5 on [31].

2 Formulation of strong coupling lattice QCD

2.1 Lattice action and its symmetry

The action on the lattice in the staggered formalism [32] is given by

$$S[U,\chi,\bar{\chi}] = S_{\rm G}[U] + S_{\rm F}[U,\chi,\bar{\chi}]\,, \tag{1}$$

which consists of the gluonic part,

$$S_{\rm G}[U] = \frac{2N_{\rm c}}{g^2}\sum_{x,\mu,\nu}\left\{1-\frac{1}{N_{\rm c}}{\rm ReTr}\,U_{\mu\nu}(x)\right\}\,, \qquad U_{\mu\nu}(x) = U_\nu^\dagger(x)U_\mu^\dagger(x+\hat{\nu})U_\nu(x+\hat{\mu})U_\mu(x)\,, \tag{2}$$

and the fermionic part with finite chemical potential,

$$\begin{aligned} S_{\rm F}[U,\chi,\bar{\chi}] = m\sum_x \bar{\chi}(x)\chi(x) &+ \frac{1}{2}\sum_x \eta_0(x)\left\{\bar{\chi}(x){\rm e}^{\mu}U_0(x)\chi(x+\hat{0}) - \bar{\chi}(x+\hat{0}){\rm e}^{-\mu}U_0^\dagger(x)\chi(x)\right\} \\ &+ \frac{1}{2}\sum_x\sum_{j=1}^{d}\eta_j(x)\left\{\bar{\chi}(x)U_j(x)\chi(x+\hat{j}) - \bar{\chi}(x+\hat{j})U_j^\dagger(x)\chi(x)\right\}\,. \end{aligned} \tag{3}$$

χ stands for the quark field in the fundamental representation of the color SU($N_{\rm c}$) group and U_μ is the SU($N_{\rm c}$) valued gauge link variable. g is the gauge coupling constant and d represents the number of spatial directions which takes 3 in reality. Later we sometimes use a notation $x=(\tau,\vec{x})$ in which τ ($\vec{x}$) represents the temporal (spatial) coordinate. $\eta_0(x)$ and $\eta_j(x)$ inherent in the staggered formalism are defined as

$$\eta_0(x) = 1\,, \qquad \eta_j(x) = (-1)^{\sum_{i=1}^{j}x_{i-1}}\,. \tag{4}$$

μ is the quark chemical potential, while the temperature is defined by $T=(aN_\tau)^{-1}$ with a being the lattice spacing and N_τ being the number of temporal sites. We will write all the dimensionful quantities in unit of a and will not write a explicitly.

The lattice action with single component staggered fermion has ${\rm U(1)_V}\times{\rm U(1)_A}$ symmetry in the chiral limit $m=0$, which is a remnant of the 4 flavor chiral symmetry in the continuum theory, defined by

$${\rm U(1)_V}: \quad \chi(x)\mapsto {\rm e}^{{\rm i}\theta_{\rm V}}\chi(x)\,, \qquad \bar{\chi}(x)\mapsto\bar{\chi}(x){\rm e}^{-{\rm i}\theta_{\rm V}} \tag{5}$$

and

$${\rm U(1)_A}: \quad \chi(x)\mapsto {\rm e}^{{\rm i}\varepsilon(x)\theta_{\rm A}}\chi(x)\,, \qquad \bar{\chi}(x)\mapsto\bar{\chi}(x){\rm e}^{{\rm i}\varepsilon(x)\theta_{\rm A}}\,. \tag{6}$$

Here $\varepsilon(x)$ is defined by

$$\varepsilon(x) = (-1)^{\sum_{\nu=0}^{d}x_\nu}\,, \tag{7}$$

which plays the similar role to that of γ_5 in the continuum theory. ${\rm U(1)_A}$ will be explicitly broken by the introduction of finite quark mass or spontaneously broken by condensation of $\langle\bar{\chi}\chi\rangle$. Note that staggered fermion's ${\rm U(1)_A}$ symmetry should not be confused with the axial U(1) symmetry in the continuum theory which is broken by the quantum effect. For $N_{\rm c}=2$, the action has a larger symmetry U(2) at $m=\mu=0$ because the color SU(2) group is pseudo-real and the action possesses Pauli-Gürsey's fermion−anti-fermion symmetry [33]. This special property for $N_{\rm c}=2$ will be revisited in the next section 3.

The main purpose of this section is to explain how to derive the effective free energy from the original action Eq. (1) systematically by accomplishing the path integrals with adopting strong coupling limit, large dimensional expansion and mean field approximation. Before addressing the computational details, we shall summarize the actual procedure:

1. Strong coupling limit $g \to \infty$ is taken. Then the gluonic part of the action $S_{\rm G}[U]$ in Eq. (2) vanishes, because it is inversely proportional to g^2. Consequently the gauge field remains only in the fermionic part (3).

2. Large dimensional $(1/d)$ expansion is employed in the spatial directions in order to facilitate the integration over the spatial gauge link variable U_j.

3. Bosonization is performed by introducing the auxiliary fields. Then the mean field approximation is adopted for the auxiliary fields so that they are regarded as spatially uniform condensates.

4. Integration with respect to χ, $\bar{\chi}$ and U_0 are accomplished exactly to result in an effective free energy written in terms of the mean field values.

2.2 Strong coupling limit and large dimensional expansion

First of all, we take the strong coupling limit $g \to \infty$ and employ the large dimensional expansion in order to perform the integration over the spatial gauge link variable U_j. Taking the strong coupling limit, the partition function in the strong coupling limit is written as

$$Z = \int \mathcal{D}[\chi, \bar{\chi}]\, \mathcal{D}[U_0]\, \mathcal{D}[U_j]\, \mathrm{e}^{-S_{\rm F}[U,\chi,\bar{\chi}]}\,. \tag{8}$$

Because χ and $\bar{\chi}$ are fermion fields, the Taylor expansion of $\mathrm{e}^{-S_{\rm F}[U,\chi,\bar{\chi}]}$ generates at most $2^{2N_{\rm c}}$ terms on each site x. Thus the integration with respect to the link variable could be performed exactly in principle. Instead, we truncate such an expansion here up to the leading order in the $1/d$ expansion. As explained soon below, the lowest order of the Taylor expansion gives the leading contribution in the $1/d$ expansion. By using the formulae for the $\mathrm{SU}(N_{\rm c})$ group integration

$$\int \mathrm{d}[U] = 1\,, \qquad \int \mathrm{d}[U]\, U_{ab} U^\dagger_{cd} = \frac{1}{N_{\rm c}} \delta_{ad}\delta_{bc}\,, \qquad \int \mathrm{d}[U]\, U_{a_1 b_1} \cdots U_{a_{N_{\rm c}} b_{N_{\rm c}}} = \frac{1}{N_{\rm c}!} \epsilon_{a_1 \cdots a_{N_{\rm c}}} \epsilon_{b_1 \cdots b_{N_{\rm c}}}\,, \tag{9}$$

we can integrate $\mathrm{e}^{-S_{\rm F}[U,\chi,\bar{\chi}]}$ with respect to U_j as follows;

$$\begin{aligned}
&\prod_x \prod_{j=1}^{d} \int \mathrm{d}[U_j(x)]\, \exp\left[-\frac{1}{2}\eta_j(x) \left\{ \bar{\chi}(x) U_j(x) \chi(x+\hat{j}) - \bar{\chi}(x+\hat{j}) U_j^\dagger(x) \chi(x) \right\} \right] \\
&= \prod_x \left[1 + \frac{N_{\rm c}}{4} \sum_{j=1}^{d} M(x) M(x+\hat{j}) \right. \\
&\qquad \left. - (-1)^{\frac{N_{\rm c}(N_{\rm c}+1)}{2}} \sum_{j=1}^{d} \left(\frac{1}{2}\eta_j(x) \right)^{N_{\rm c}} \left\{ \bar{B}(x) B(x+\hat{j}) + (-1)^{N_{\rm c}} \bar{B}(x+\hat{j}) B(x) \right\} + \cdots \right] \\
&= \exp\left[\sum_{x,y} M(x) V_{\rm M}(x,y) M(y) + \sum_{x,y} \bar{B}(x) V_{\rm B}(x,y) B(y) \right] + \cdots\,,
\end{aligned} \tag{10}$$

where $M(x)$ and $B(x)$, $\bar{B}(x)$ are the mesonic and baryonic composites defined respectively as

$$\begin{aligned}
M(x) &= \frac{1}{N_{\rm c}} \delta_{ab}\, \bar{\chi}^a(x) \chi^b(x)\,, \\
B(x) &= \frac{1}{N_{\rm c}!} \epsilon_{a_1 \cdots a_{N_{\rm c}}}\, \chi^{a_1}(x) \cdots \chi^{a_{N_{\rm c}}}(x)\,, \quad \bar{B}(x) = -\frac{1}{N_{\rm c}!} \epsilon_{b_1 \cdots b_{N_{\rm c}}}\, \bar{\chi}^{b_1}(x) \bar{\chi}^{b_{N_{\rm c}}}(x)\,,
\end{aligned} \tag{11}$$

and their propagators in the spatial directions are given by

$$
\begin{aligned}
V_{\rm M}(x,y) &= \frac{N_{\rm c}}{4}\sum_{j=1}^{d}\left(\delta_{y,x+\hat{j}}+\delta_{y,x-\hat{j}}\right)\,,\\
V_{\rm B}(x,y) &= -\frac{(-1)^{N_{\rm c}(N_{\rm c}+1)/2}}{2^{N_{\rm c}}}\sum_{j=1}^{d}\left[\eta_j(x)\right]^{N_{\rm c}}\left[\delta_{y,x+\hat{j}}+(-1)^{N_{\rm c}}\delta_{y,x-\hat{j}}\right]\,.
\end{aligned}
\tag{12}
$$

The Latin indices $a, b, \ldots$ are summed over from 1 to $N_{\rm c}$ in the color space.

The reason why the lowest order terms of the Taylor expansion of $\mathrm{e}^{-S_{\rm F}[U,\chi,\bar{\chi}]}$ correspond to the leading contributions of the $1/d$ expansion can be understood by changing the normalization of quark field as $M(x) \to \tilde{M}(x)/\sqrt{d}$ so that the mesonic propagator $\tilde{V}_{\rm M}(x,y) = V_{\rm M}(x,y)/d$ becomes O(1) in the large d limit. As a result , because the higher order terms in the Taylor expansion contain more quark fields χ and $\bar{\chi}$, they are associated with more $1/d^{1/4}$ and then vanish in the large d limit. To clarify the argument, we consider the baryonic term in Eq. (10). Changing the normalization of quark fields $\chi, \bar{\chi}$ to the one suitable for $1/d$ expansion, the baryonic term becomes

$$
\bar{B}(x)V_{\rm B}(x,y)B(y) \to \frac{1}{d^{N_{\rm c}/2-1}}\tilde{\bar{B}}(x)\tilde{V}_{\rm B}(x,y)\tilde{B}(y)\,,
\tag{13}
$$

where $\tilde{V}_{\rm B}(x,y) = V_{\rm B}(x,y)/d$. Therefore the baryonic term turns out to be of higher in the $1/d$ expansion as long as $N_{\rm c} \geq 3$ because $\tilde{V}_{\rm B}(x,y)$ is $O(1)$ in the large d limit. For $N_{\rm c} = 2$, however, the baryonic term contributes to the same order as the mesonic one and it can never be neglected in terms of large dimensional expansion. The resultant action (10) describes the nearest neighbor interactions of the mesonic composite $M(x)$ and of the baryonic composites $B(x)$ and $\bar{B}(x)$.

2.3 Bosonization with the auxiliary fields

In order to accomplish the remaining integrations over $\chi, \bar{\chi}$ and U_0, we perform the bosonization and mean field approximation. The mesonic term in Eq. (10) is the four fermion interaction, we may linearize it by introducing the auxiliary field $\sigma(x)$ (chiral field) with a standard Gaussian technique;

$$
\exp\left[\sum_{x,y}M(x)V_{\rm M}(x,y)M(y)\right] = \int\mathcal{D}[\sigma]\,\exp\left[-\sum_{x,y}\left\{\sigma(x)V_{\rm M}(x,y)\sigma(y)+2\sigma(x)V_{\rm M}(x,y)M(y)\right\}\right]\,.
\tag{14}
$$

For $N_{\rm c} = 2$ case, the baryonic term is also four fermion interaction and can be linearized by introducing the boson fields $\Delta(x)$ and $\Delta^*(x)$ (diquark fields) as

$$
\begin{aligned}
&\exp\left[\sum_{x,y}\bar{B}(x)V_{\rm B}(x,y)B(y)\right]\\
&\quad=\int\mathcal{D}[\Delta,\Delta^*]\,\exp\left[-\sum_{x,y}\left\{\Delta^*(x)V_{\rm B}(x,y)\Delta(y)-\Delta^*(x)V_{\rm B}(x,y)B(y)-\bar{B}(x)V_{\rm B}(x,y)\Delta(y)\right\}\right]\,.
\end{aligned}
\tag{15}
$$

From the above transformations, it is easy to show the relation

$$
\langle\sigma(x)\rangle = -\langle M(x)\rangle\,,\qquad \langle\Delta(x)\rangle = \langle B(x)\rangle\,,\quad \langle\Delta^*(x)\rangle = \left\langle\bar{B}(x)\right\rangle\,,
\tag{16}
$$

where we have chosen the definition of the field $\sigma(x)$ so that the sign of $\langle\sigma(x)\rangle$ becomes positive for $m > 0$. Consequently, we obtain the following partition function in the leading order of strong coupling

and large dimensions;

$$Z = \int \mathcal{D}[\chi, \bar{\chi}]\, \mathcal{D}[U_0]\, \mathcal{D}[\sigma]\, \mathcal{D}[\Delta, \Delta^*]\, \mathrm{e}^{-S'[U_0, \chi, \bar{\chi}, \sigma, \Delta]}\,, \tag{17}$$

where

$$\begin{aligned} S'[U, \chi, \bar{\chi}, \sigma, \Delta] = m \sum_x \bar{\chi}(x)\chi(x) + \frac{1}{2}\sum_x \eta_0(x) \left\{ \bar{\chi}(x)\mathrm{e}^{\mu} U_0(x) \chi(x+\hat{0}) - \bar{\chi}(x+\hat{0})\mathrm{e}^{-\mu} U_0^\dagger(x)\chi(x) \right\} \\ + \sum_{x,y} \{\sigma(x) V_{\mathrm{M}}(x,y)\sigma(y) + 2\sigma(x) V_{\mathrm{M}}(x,y) M(y)\} \\ + \delta_{N_{\mathrm{c}},2} \sum_{x,y} \left\{ \Delta^*(x) V_{\mathrm{B}}(x,y)\Delta(y) - \Delta^*(x) V_{\mathrm{B}}(x,y) B(y) - \bar{B}(x) V_{\mathrm{B}}(x,y)\Delta(y) \right\}. \end{aligned} \tag{18}$$

Demanding the invariance of the above action under the $\mathrm{U}(1)_{\mathrm{V}}$ or $\mathrm{U}(1)_{\mathrm{A}}$ transformation defined respectively by (5) and (6), we can assign the transformation for the chiral field as

$$\mathrm{U}(1)_{\mathrm{V}}: \quad \sigma(x) \mapsto \sigma(x) \qquad \text{and} \qquad \mathrm{U}(1)_{\mathrm{A}}: \quad \sigma(x) \mapsto \mathrm{e}^{2\mathrm{i}\varepsilon(x)\theta_{\mathrm{A}}} \sigma(x)\,. \tag{19}$$

Then the finite vacuum expectation value of $\sigma(x)$ means the spontaneous breakdown of chiral symmetry $\mathrm{U}_{\mathrm{A}}(1)$. In the same way, we can determine the transformation for the diquark fields for $N_{\mathrm{c}} = 2$ as

$$\mathrm{U}(1)_{\mathrm{V}}: \quad \Delta(x) \mapsto \mathrm{e}^{2\mathrm{i}\theta_{\mathrm{V}}} \Delta(x) \qquad \text{and} \qquad \Delta^*(x) \mapsto \mathrm{e}^{-2\mathrm{i}\theta_{\mathrm{V}}} \Delta^*(x)\,, \tag{20}$$

$$\mathrm{U}(1)_{\mathrm{A}}: \quad \Delta(x) \mapsto \mathrm{e}^{2\mathrm{i}\varepsilon(x)\theta_{\mathrm{A}}} \Delta(x) \qquad \text{and} \qquad \Delta^*(x) \mapsto \mathrm{e}^{2\mathrm{i}\varepsilon(x)\theta_{\mathrm{A}}} \Delta^*(x)\,. \tag{21}$$

Then the finite vacuum expectation value of $|\Delta(x)|$ means the spontaneous breakdown of the chiral symmetry and the baryon number conservation $\mathrm{U}_{\mathrm{V}}(1)$, which leads to the diquark superfluidity.

What we have to do next to derive the effective free energy written by the above vacuum expectation values is a mean field approximation. Namely, we replace the auxiliary fields $\sigma(x)$ and $\Delta(x)$ by the constant mean field values and ignore any fluctuations around them. Then since $S'[U_0, \chi, \bar{\chi}; \sigma, \Delta]$ becomes in a bilinear form with respect to the quark fields χ and $\bar{\chi}$, we can integrate out them immediately. The integration with respect to U_0, which seems to be tough at first glance, turns out to be feasible. The actual procedures of the mean field approximation and the integration over $\chi, \bar{\chi}$ and U_0 will be demonstrated for $N_{\mathrm{c}} = 2$ case and $N_{\mathrm{c}} \geq 3$ case separately in the succeeding sections.

3 QCD ($N_c = 2, N_f = 4$) with finite baryon density

In this section, we consider the case of $N_c = 2$, which is called 2-color QCD in this section. One of the major differences between 2-color QCD and $SU_c(3)$ QCD lies in the fact that the color-singlet baryons are bosons in the former. This implies that the ground state of the 2-color system at finite baryon density in the color-confined phase is an interacting boson system, i.e. a Bose liquid, although the quark Fermi liquid may be realized at high baryon density in the color-deconfined phase. How this Bose liquid changes its character as a function of the temperature T, the quark chemical potential μ_B and the quark mass m is an interesting question by itself and may also give a hint to understand physics of the color superconductivity in 3-color QCD in which the crossover from the Bose-Einstein condensate of tightly bound quark pairs to the BCS type condensate of loosely bound Cooper pairs may take place [34].

3.1 Pauli-Gürsey symmetry

Before to address the derivation of an effective free energy, here we shall consider the symmetry of 2-color QCD and its breaking pattern. As we have already mentioned in Sec. 2.1, the lattice action (3) has $U(2)$ symmetry at $m = \mu = 0$ for $N_c = 2$. In order to see this symmetry explicitly, we rearrange Eq. (3) by using the Grassmann nature of $\chi, \bar{\chi}$, the fact that $\eta_\mu(x) = \eta_\mu(x \pm \hat{\mu})$ and the property $\tau_2 U_\mu \tau_2 = U_\mu^*$ where τ_2 is a Pauli matrix. Then we rewrite the action in the chiral limit $m = 0$ as follows [13];

$$S_F[U,\chi,\bar{\chi}] = \frac{1}{2}\sum_{x:\text{even}} \eta_0(x)\left[\bar{\Psi}(x-\hat{0})\begin{pmatrix} e^{\mu} & 0 \\ 0 & e^{-\mu}\end{pmatrix} U_0(x-\hat{0})\Psi(x) - \bar{\Psi}(x+\hat{0})\begin{pmatrix} e^{-\mu} & 0 \\ 0 & e^{\mu}\end{pmatrix} U_0^\dagger(x)\Psi(x)\right] + \frac{1}{2}\sum_{x:\text{even}}\sum_{j=1}^{d}\eta_j(x)\left[\bar{\Psi}(x-\hat{j})U_j(x-\hat{j})\Psi(x) - \bar{\Psi}(x+\hat{j})U_j^\dagger(x)\Psi(x)\right], \tag{22}$$

where

$$\bar{\Psi}(x:\text{odd}) = \left(\bar{\chi}(x), -\tau_2\chi^t(x)\right) \qquad \text{and} \qquad \Psi(x:\text{even}) = \begin{pmatrix}\chi(x) \\ -\tau_2\bar{\chi}^t(x)\end{pmatrix}. \tag{23}$$

The summation is only over even sites defined by where $\varepsilon(x) = 1$ and the field $\Psi(x)$ is defined only on even sites and $\bar{\Psi}(x)$ on odd sites ($\varepsilon(x) = -1$). As we can see manifestly, the action at zero chemical potential $\mu = 0$ has a global $U(2)$ symmetry defined by

$$\Psi(x) \mapsto W\Psi(x) \qquad \text{and} \qquad \bar{\Psi}(x) \mapsto \bar{\Psi}(x)W^\dagger, \qquad \text{with} \quad W \in \mathrm{U}(2). \tag{24}$$

This larger symmetry is a special feature for 2-color QCD and sometimes called as Pauli-Gürsey symmetry which mixes fermions with anti-fermions. This is nothing but the consequence of the pseudo-reality of the color SU(2) group $\tau_2 U_\mu \tau_2 = U_\mu^*$.

Introduction of finite chemical potential reduces the U(2) symmetry to the usual $\mathrm{U_V}(1) \times \mathrm{U_A}(1)$ symmetry defined by Eqs. (5) and (6) and finite quark mass breaks it to the $\mathrm{U_V}(1)$ symmetry. As explained in Sec. 2.3, the formation of the diquark condensation $\langle\chi\chi\rangle$ spontaneously breaks the $\mathrm{U_V}(1)$ and $\mathrm{U_A}(1)$ symmetry and lead to baryon superfluidity. The symmetries realized in various circumstances and their breaking patterns by the diquark condensation are summarized in Table 1. In the succeeding subsections, we derive the effective action in terms of the chiral and diquark fields and analyze the phase structure of 2-color QCD as functions of temperature, chemical potential and quark mass.

	$m = 0$	$m \neq 0$
$\mu = 0$	U(2) broken to U(1) with 3 NG modes	$U_V(1)$ not broken
$\mu \neq 0$	$U_V(1) \times U_A(1)$ totally broken with 2 NG modes	$U_V(1)$ totally broken with 1 NG mode

Table 1: Symmetry realized in the lattice action for $N_c = 2$ with one species of staggered fermion. Possible symmetry breaking patterns by the diquark condensation and the number of Nambu-Goldstone (NG) modes are also listed.

3.2 Derivation of an effective action

3.2.1 Mean field approximation

We start from the action in Eq.(18) which is obtained after the strong coupling limit, $1/d$ expansion and bosonization. We replace the auxiliary fields $\sigma(x)$ and $\Delta(x)$ in Eq.(18) by the constant mean field values σ and Δ and ignore any fluctuations around them. It is obvious from Eq. (16) that σ should be identified with the chiral condensate and Δ be the diquark condensate:

$$\sigma = -\langle M(x) \rangle \ , \qquad \Delta = \langle B(x) \rangle \ , \quad \Delta^* = \left\langle \bar{B}(x) \right\rangle \ . \tag{25}$$

Then we can write the partition function as

$$Z = \int \mathcal{D}[U_0]\, \mathcal{D}[\chi, \bar{\chi}]\, \mathrm{e}^{-S'[U_0, \chi, \bar{\chi}; \sigma, \Delta]} \, , \tag{26}$$

with

$$\begin{aligned} S'[U_0, \chi, \bar{\chi}; \sigma, \Delta] = \sum_x \Bigg[& m\bar{\chi}(x)\chi(x) + \frac{1}{2}\left\{ \bar{\chi}(x)\mathrm{e}^{\mu} U_0(x) \chi(x+\hat{0}) - \bar{\chi}(x+\hat{0})\mathrm{e}^{-\mu} U_0^\dagger(x)\chi(x) \right\} \\ & + \frac{d}{2}\sigma^2 + \frac{d}{2}|\Delta|^2 + d\,\sigma M(x) - \frac{d}{2}\Delta^* B(x) - \frac{d}{2}\Delta \bar{B}(x) \Bigg] \ . \end{aligned} \tag{27}$$

Since $S'[U_0, \chi, \bar{\chi}; \sigma, \Delta]$ is in a bilinear form with respect to the quark fields χ and $\bar{\chi}$, we can integrate out them immediately. Then the integration with respect to U_0 also can be performed as shown below.

3.2.2 Integrations over χ, $\bar{\chi}$ and U_0

In order to complete the remaining integrals, we adopt a particular gauge in which $U_0(\tau, \vec{x})$ is diagonal and independent of τ (often called the Polyakov gauge),

$$U_0(\tau, \vec{x}) = \mathrm{diag}\left(\mathrm{e}^{\mathrm{i}\phi_1(\vec{x})/N_\tau}, \mathrm{e}^{\mathrm{i}\phi_2(\vec{x})/N_\tau} \right) \ , \qquad \text{with} \quad \phi_1(\vec{x}) = -\phi_2(\vec{x}) \, . \tag{28}$$

Also we make a partial Fourier transformation for the quark fields;

$$\chi(\tau, \vec{x}) = \frac{1}{\sqrt{N_\tau}} \sum_{n=1}^{N_\tau} \mathrm{e}^{\mathrm{i}k_n \tau} \tilde{\chi}(n, \vec{x}) \, , \quad \bar{\chi}(\tau, \vec{x}) = \frac{1}{\sqrt{N_\tau}} \sum_{n=1}^{N_\tau} \mathrm{e}^{-\mathrm{i}k_n \tau} \tilde{\bar{\chi}}(n, \vec{x}) \, , \qquad k_n = 2\pi \frac{(n - \frac{1}{2})}{N_\tau} \, . \tag{29}$$

The anti-periodic condition in the temporal direction , $\chi(\tau + N_\tau, \vec{x}) = -\chi(\tau, \vec{x})$, is satisfied owing to the fermionic Matsubara frequency k_n.

Substituting Eqs. (28) and (29) into the action (27) and taking the summation over τ, we reach the action in a Nambu-Gor'kov representation;

$$S'[\phi,\chi,\bar{\chi};\sigma,\Delta] = \sum_x \left(\frac{d}{2}\sigma^2 + \frac{d}{2}|\Delta|^2\right) - \frac{1}{2}\sum_{\vec{x}}\sum_{m,n}[X^a(m,\vec{x})]^{\rm t}\, G^{-1}_{ab}(m,n;\phi(\vec{x}))\, X^b(n,\vec{x})\,, \tag{30}$$

where

$$X^a(n,\vec{x}) = \begin{pmatrix}\tilde{\chi}^a(n,\vec{x})\\ \tilde{\bar{\chi}}^a(n,\vec{x})\end{pmatrix}, \tag{31}$$

and

$$G^{-1}_{ab}(m,n;\phi(\vec{x})) \tag{32}$$
$$= \begin{pmatrix} \dfrac{d}{2}\Delta^*\,\delta_{m,N_\tau-n+1}\epsilon_{ab} & \left[M + {\rm i}\sin\left(k_m + \dfrac{\phi_a(\vec{x})}{N_\tau} - {\rm i}\mu\right)\right]\delta_{mn}\delta_{ab} \\ -\left[M + {\rm i}\sin\left(k_m + \dfrac{\phi_a(\vec{x})}{N_\tau} - {\rm i}\mu\right)\right]\delta_{mn}\delta_{ab} & -\dfrac{d}{2}\Delta\,\delta_{m,N_\tau-n+1}\epsilon_{ab}\end{pmatrix}.$$

The indices a and b run from 1 through 2 in the color space. M denotes the dynamical quark mass (to be distinguished from the mesonic composite $M(x)$) defined by

$$M = m + \frac{d}{2}\sigma\,. \tag{33}$$

We can perform the Grassmann integration over χ and $\bar{\chi}$ as [35]

$$\int \mathcal{D}[\chi,\bar{\chi}]\,{\rm e}^{X^{\rm t}G^{-1}X} = \prod_{\vec{x}}\sqrt{{\rm Det}\left[G^{-1}_{ab}(m,n;\phi(\vec{x}))\right]}\,. \tag{34}$$

Det stands for the determinant with respect to the color indices and the Matsubara frequencies. The square root of the determinant may be simplified as

$$\sqrt{{\rm Det}[G^{-1}]} = \prod_{n=1}^{N_\tau}\left[\left(\frac{d}{2}\right)^2|\Delta|^2 + \{M + {\rm i}\sin\left(k_n + \phi/N_\tau - {\rm i}\mu\right)\}\cdot\{M - {\rm i}\sin\left(k_n + \phi/N_\tau + {\rm i}\mu\right)\}\right], \tag{35}$$

where $\phi_1 = -\phi_2 = \phi$ is substituted. The product with respect to n can be performed using a technique similar to that in the calculation of the free energy in finite-temperature field theory in the continuum. The details of the calculation is given in Appendix A.1. The result turns out to be a rather simple form,

$$\sqrt{{\rm Det}\left[G^{-1}_{ab}(m,n;\phi)\right]} = (2\cos\phi + 2\cosh N_\tau E_-)\cdot(2\cos\phi + 2\cosh N_\tau E_+)\,. \tag{36}$$

Here $E_\pm$ are the excitation energy of quasi-quarks and anti-quasi-quarks,

$$E_\pm = {\rm arccosh}\left(\sqrt{(1+M^2)\cosh^2(\mu_{\rm B}/2) + (d/2)^2|\Delta|^2} \pm M\sinh(\mu_{\rm B}/2)\right). \tag{37}$$

with the dynamical quark mass M defined in Eq. (33) We have defined the baryon chemical potential $\mu_{\rm B}$ as $\mu_{\rm B} = 2\mu$.

Finally, all we have to do is to integrate this resultant determinant with respect to U_0, or ϕ, to derive the effective action;

$$S_{\rm eff}[\sigma,\Delta] = -\log Z = \sum_x\left(\frac{d}{2}\sigma^2 + \frac{d}{2}|\Delta|^2\right) - \sum_{\vec{x}}\log\left\{\int\frac{{\rm d}\phi(\vec{x})}{2\pi}\sin^2\phi(\vec{x})\sqrt{{\rm Det}\left[G^{-1}_{ab}(m,n;\phi(\vec{x}))\right]}\right\}, \tag{38}$$

where we have used the SU(2) Haar measure in the Polyakov gauge (28),

$$\int \mathcal{D}[U_0] = \prod_{\vec{x}} \int_{-\pi}^{\pi} \frac{\mathrm{d}\phi(\vec{x})}{2\pi} \sin^2 \phi(\vec{x}) \Bigg|_{\phi(\vec{x})=\phi_1(\vec{x})=-\phi_2(\vec{x})} . \tag{39}$$

The U_0 integration projects out the color singlet pairing of quarks and anti-quarks among arbitrary excitations in the determinant. Thus what excites thermally is no longer single quarks, but color singlet mesons or diquarks. In this sense, the strong coupling limit in 2-color QCD inevitably leads to the confined boson system.

Then Eqs. (36), (38) and (39) immediately yield the effective free energy;

$$F_{\mathrm{eff}}[\sigma, \Delta] = S_{\mathrm{eff}}/(\textstyle\sum_x) = \frac{d}{2}\sigma^2 + \frac{d}{2}|\Delta|^2 - T \log \left\{1 + 4\cosh\left(E_+/T\right) \cdot \cosh\left(E_-/T\right)\right\} , \tag{40}$$

where we have rewritten N_τ in terms of the temperature $T(= 1/N_\tau)$.

Although the quasi-quark energy $E_\pm$ given in Eq. (37) takes a complicated form, $E_\pm$ is reduced to a simple expression in the *naive* continuum $a \to 0$ with a being the lattice spacing. Assuming Ma, Δa, $\mu a \ll 1$ in this limit, $E_\pm$ amounts to a familiar form in the continuous space-time,

$$E_\pm \sim \operatorname{arccosh}\left(\sqrt{1 + M^2 + \left(\mu_{\mathrm{B}}/2\right)^2 + (d/2)^2|\Delta|^2} \pm M\mu_{\mathrm{B}}/2\right) \to \sqrt{(M \pm \mu_{\mathrm{B}}/2)^2 + (d/2)^2|\Delta|^2} . \tag{41}$$

The quasi-quarks are static in this framework because of the mean field approximation.

3.3 Analytical results on the phase structure

3.3.1 Case in the chiral limit

In the chiral limit $m = 0$ with zero chemical potential $\mu_{\mathrm{B}} = 0$, the free energy in the mean field approximation given in Eq. (40) is a function only in terms of $\sigma^2 + |\Delta|^2$. As a result, the free energy is invariant under the transformation mixing the chiral condensate with the diquark one. This corresponds to a subgroup of the U(2) symmetry of the original action at $m = \mu_{\mathrm{B}} = 0$ in Table 1. Because of this symmetry, the chiral condensate is indistinguishable from the diquark condensate for $m = \mu_{\mathrm{B}} = 0$, so that a state with finite σ can be arbitrarily transformed to a state with finite Δ.

Finite μ_{B} would act on the free energy as an external field tending to make the diquark condensation favored. Consequently even an infinitesimal introduction of μ_{B} leads to the diquark condensation phase with zero chiral condensate in the chiral limit. This is a peculiar feature of 2-color QCD and is in a sharp contrast to the 3-color QCD. In fact, we can prove that the minimizing condition for our $F_{\mathrm{eff}}[\sigma, \Delta]$ does not allow non-zero σ at any T and μ_{B} in the chiral limit. See Appendix B for the proof.

Taking the fact that σ vanishes in the chiral limit for granted, the free energy is simply written as

$$F_{\mathrm{eff}}[\Delta] = \frac{d}{2}|\Delta|^2 - T \log \left\{1 + 4\cosh^2\left(E_0/T\right)\right\} , \qquad E_0 = \operatorname{arccosh}\left(\sqrt{(d/2)^2|\Delta|^2 + \cosh^2\left(\mu_{\mathrm{B}}/2\right)}\right) . \tag{42}$$

Assuming that the finite temperature phase transition with fixed μ_{B} is of second order, which will be confirmed numerically later, the critical temperature T_{c} may be determined by expanding $F_{\mathrm{eff}}[\Delta]$ in terms of $|\Delta|^2$ and extracting the point where the coefficient of $|\Delta|^2$ changes its sign. Since the expansion reads

$$F_{\mathrm{eff}}[\Delta] = -T \log \left\{3 + 2\cosh\left(\mu_{\mathrm{B}}/T\right)\right\} + \left\{\frac{d}{2} - \frac{d^2}{3 + 2\cosh\left(\mu_{\mathrm{B}}/T\right)} \frac{\sinh\left(\mu_{\mathrm{B}}/T\right)}{\sinh \mu_{\mathrm{B}}}\right\} |\Delta|^2 + \mathrm{O}\left(|\Delta|^4\right) , \tag{43}$$

one finds

$$T_{\rm c}(\mu) = \mu_{\rm B} \left\{ \mathrm{arccosh} \left(\frac{3\sinh^2\mu_{\rm B} + d\sqrt{4d^2 + 5\sinh^2\mu_{\rm B}}}{2d^2 - 2\sinh^2\mu_{\rm B}} \right) \right\}^{-1} . \tag{44}$$

The values of $T_{\rm c}(\mu_{\rm B})$ for two typical cases are

$$T_{\rm c}(\mu_{\rm B}=0) = \frac{6}{5}, \qquad T_{\rm c}(\mu_{\rm B} = \mu_{\rm B}^{\rm cri} = \mathrm{arcsinh}\, d \simeq 1.82) = 0 \tag{45}$$

for $d = 3$. T_c is a monotonously decreasing function of $\mu_{\rm B}$ connecting the above two points. This will be discussed later in Sec. 3.4 together with the case at finite m.

It is interesting to calculate the baryon density $\rho_{\rm B}$ which is defined as

$$\rho_{\rm B}(\mu_{\rm B}, T) = -\frac{\partial F_{\rm eff}}{\partial \mu_{\rm B}} = \frac{8\cosh(E_0/T)\sinh(E_0/T)}{1 + 4\cosh^2(E_0/T)} \cdot \frac{\partial E_0}{\partial \mu_{\rm B}}, \tag{46}$$

where E_0 is the quasi-quark mass in the chiral limit defined in Eq. (42). Although the above expression seems to be a little complicated, it can be simplified by using the gap equation;

$$0 = \frac{\partial F_{\rm eff}}{\partial \Delta^*} = \frac{d}{2}\Delta - \frac{8\cosh(E_0/T)\sinh(E_0/T)}{1 + 4\cosh^2(E_0/T)} \cdot \frac{(d/2)^2\Delta}{\sinh\mu_{\rm B}} \cdot 2\frac{\partial E_0}{\partial \mu_{\rm B}} . \tag{47}$$

In general the gap equation may have two solutions, $\Delta = 0$ and $\Delta \neq 0$. The former (the latter) is the solution to minimize the free energy for $T \geq T_{\rm c}(\mu)$ ($T < T_{\rm c}(\mu)$). It can be alternatively said that the former (the latter) is the solution for $\mu_{\rm B} \geq \mu_{\rm B}^{\rm cri}(T)$ ($\mu_{\rm B} \leq \mu_{\rm B}^{\rm cri}(T)$) with the critical chemical potential $\mu_{\rm B}^{\rm cri}$ as a solution of Eq. (44) in terms of μ.

By eliminating most of the complicated part of Eq. (46) by means of the gap equation (47), we have the following expressions;

$$\rho_{\rm B}(\mu_{\rm B}, T) = \begin{cases} (\sinh\mu_{\rm B})/d & \text{for} \quad \mu_{\rm B} < \mu_{\rm B}^{\rm cri}(T) \quad (\Delta \neq 0), \\ \dfrac{2\sinh(\mu_{\rm B}/T)}{3 + 2\cosh(\mu_{\rm B}/T)} & \text{for} \quad \mu_{\rm B} \geq \mu_{\rm B}^{\rm cri}(T) \quad (\Delta = 0). \end{cases} \tag{48}$$

At zero temperature, Eq. (48) is reduced to

$$\rho_{\rm B}(\mu_{\rm B}, T=0) = \begin{cases} (\sinh\mu_{\rm B})/d & \text{for} \quad \mu_{\rm B} < \mu_{\rm B}^{\rm cri}(T=0), \\ 1 & \text{for} \quad \mu_{\rm B} \geq \mu_{\rm B}^{\rm cri}(T=0) \end{cases} \tag{49}$$

with

$$\mu_{\rm B}^{\rm cri}(T=0) = \mathrm{arcsinh}\, d, \tag{50}$$

at which the baryon density $\rho_{\rm B}$ gets to be saturated to one. Note that quarks on each lattice site have only two degrees of freedom in the color space because the spin and flavor degrees of freedom are dispersed on the staggered lattice sites. Therefore "one" is the maximum number of baryon placed on each lattice site due to the Pauli exclusion principle of constituent quarks.

3.3.2 Case at zero temperature with finite m

Even a small quark mass could modify the phase structure substantially from that given above for chiral limit. This is because the pion, that is the Nambu-Goldstone mode associated with the chiral $\mathrm{U_A}(1)$ symmetry breaking, comes to have a finite mass, $m_\pi \propto m^{1/2}$. As a result, as far as the baryon

chemical potential is smaller than a threshold value, the vacuum is empty and the diquark condensate vanishes; $\rho_B(\mu_B, T = 0) = 0$ and $\Delta(\mu_B, T = 0) = 0$.

To clarify such threshold effects in more detail, let us now focus our attention on the $T = 0$ system with finite m. We derive analytical formulae for lower-critical chemical potential $\mu_c^{\rm low}$ at which Δ starts to be non-vanishing and the upper-critical chemical potential $\mu_c^{\rm up}$ at which Δ ceases to be non-vanishing.

The free energy at $T = 0$ with finite m takes a simple form;

$$F_{\rm eff}[\sigma, \Delta] = \frac{d}{2}\sigma^2 + \frac{d}{2}|\Delta|^2 - (E_+ + E_-) \ . \tag{51}$$

The expansion of $F_{\rm eff}[\sigma, \Delta]$ in terms of $|\Delta|^2$ near the threshold gives a condition to determine the critical chemical potential $\mu_B^{\rm cri}$,

$$\frac{d}{2} - \frac{d^2}{8\cosh E \cosh(\mu_B^{\rm cri}/2)} \left(\frac{1}{\sinh(E + \mu_B^{\rm cri}/2)} + \frac{1}{|\sinh(E - \mu_B^{\rm cri}/2)|} \right) = 0 \, , \tag{52}$$

where $E = {\rm arccosh}(\sqrt{1 + M^2})$ and $M = m + d\sigma/2$ as defined in Eq. (33). In Eq. (52) the dynamical mass M, or σ, is determined by the condition to minimize the free energy at the threshold. We can reduce that free energy much more by putting $\Delta = 0$,

$$F_{\rm eff}[\sigma] = \frac{d}{2}\sigma^2 - (E + \mu_B/2 + |E - \mu_B/2|) \ . \tag{53}$$

The stationary condition of the free energy $F_{\rm eff}[\sigma]$ with respect to σ yields the following chiral gap equations;

$$\frac{2}{d}(M - m) = \begin{cases} (1 + M^2)^{-1/2} & \text{for} \quad \mu_B < 2E \, , \\ 0 & \text{for} \quad \mu_B \geq 2E \, . \end{cases} \tag{54}$$

Combining Eq. (52) and Eq. (54), we find

$$\mu_B^{\rm cri} = \begin{cases} \mu_c^{\rm low} = 2\,{\rm arccosh}\sqrt{1 + mM} & \text{for} \quad \mu_B < 2E \, , \\ \mu_c^{\rm up} = 2\,{\rm arccosh}\sqrt{1 + K^2} & \text{for} \quad \mu_B \geq 2E \, , \end{cases} \tag{55}$$

where we define K as the solution of the equation,

$$\frac{2}{d}\left(K - \frac{m^2}{K} \right) = (1 + K^2)^{-1/2} \, . \tag{56}$$

With finite m at $T = 0$, the empty vacuum gives $\rho_B = 0$ and $\Delta = 0$ as long as $\mu_B < \mu_c^{\rm low}$. On the other hand, the non-vanishing value of Δ is possible for $\mu_c^{\rm low} \leq \mu_B \leq \mu_c^{\rm up}$. For $\mu_B > \mu_c^{\rm up}$, the saturation of the baryon density occurs leading to $\rho_B = 1$ and $\Delta = 0$. These behaviors will be confirmed numerically in Sec. 3.4.

Note that we have not assumed the quark mass m to be small, which is in contrast to the approaches based on chiral perturbation theory [36, 37]. Therefore, Eq. (55) can relate the critical chemical potentials to arbitrary values of m. For sufficiently small m, we have a relation;

$$\mu_c^{\rm low} = 2\, m^{1/2} \cdot \left\{ \frac{(1 + d^2)^{1/2} - 1}{2} \right\}^{1/4} , \qquad \mu_c^{\rm up} = {\rm arcsinh}\, d \, . \tag{57}$$

The former may be rewritten as $\mu_c^{\rm low} = m_\pi$ with m_π obtained from the excitation spectrum in the vacuum [38] up to the leading order of the $1/d$ expansion. This observation is consistent with the

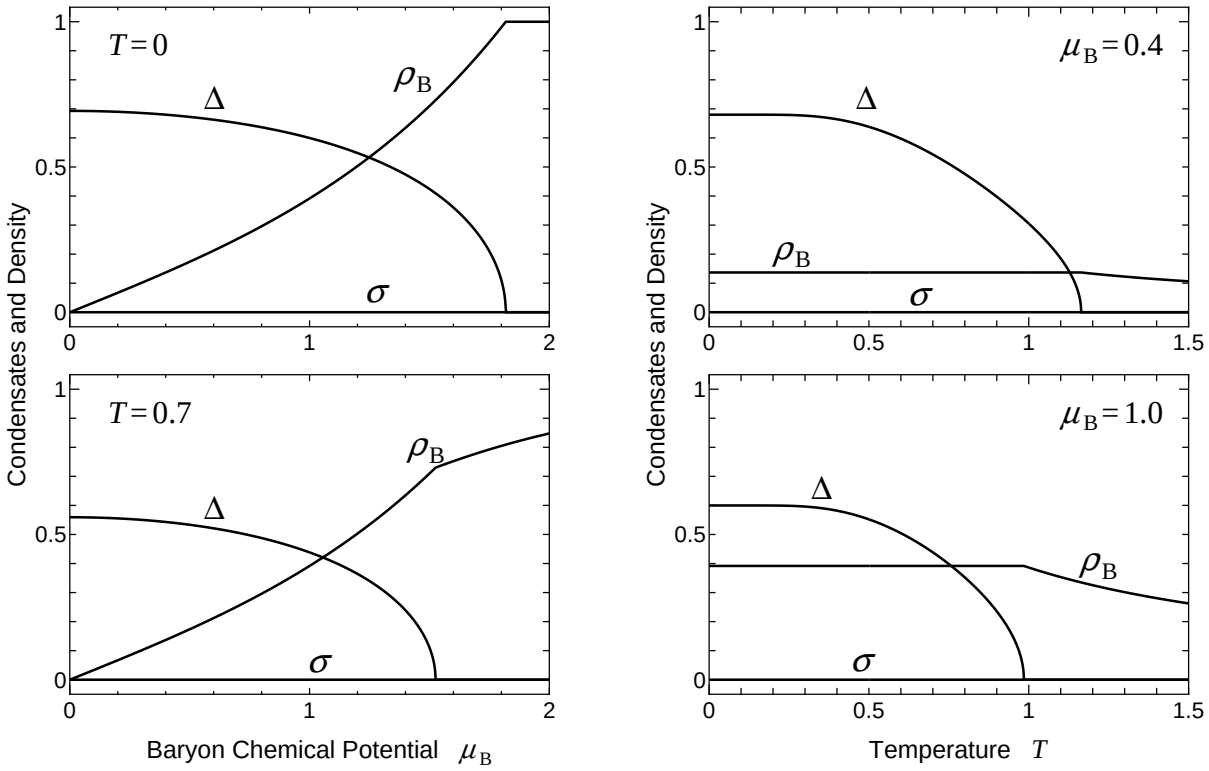

Figure 1: Chiral condensate σ, diquark condensate Δ, and the baryon density $\rho_{\rm B}$ for $m = 0$ with $d = 3$. In the left panels they are plotted as functions of the chemical potential $\mu_{\rm B}$ for two typical values of temperature. In the right panels, they are plotted as functions of temperature T for two typical values of $\mu_{\rm B}$. All the dimensionful quantities are in unit of the lattice spacing a, which is implicitly understood in all the figures in this section.

discussion given in [36]. The latter relation is simply rewritten as $\mu_{\rm c}^{\rm up} = \mu_{\rm c}(T = 0)$ with $\mu_{\rm c}(T = 0)$ defined in Eq.(50).

For sufficiently large m, we find asymptotically,

$$\mu_{\rm c}^{\rm low} \simeq \mu_{\rm c}^{\rm up} \simeq 2\,{\rm arccosh}\, m\,. \tag{58}$$

This is because $M \simeq K \simeq m$ for large m as is evident from Eqs. (54) and (56).

3.4 Numerical results on the phase structure

In this section, we determine the chiral condensate σ and the diquark condensate Δ numerically by minimizing the effective free energy in Eq. (40). The baryon density $\rho_{\rm B}$ is also calculated numerically. The results are shown in Figs. 1 and 2 for $m = 0$ and $m = 0.02$, respectively. The phase diagrams of the system in the T-$\mu_{\rm B}$ plane, in the $\mu_{\rm B}$-m plane and in the three dimensional T-$\mu_{\rm B}$-m space are also shown in Figs. 3, 4 and 5, respectively.

3.4.1 Case for $m = 0$

Let us first consider the diquark condensate and the baryon density as functions of $\mu_{\rm B}$ and T shown in the four panels of Fig. 1. (Note that the chiral condensate is always zero in the chiral limit as we have proved in Appendix B.)

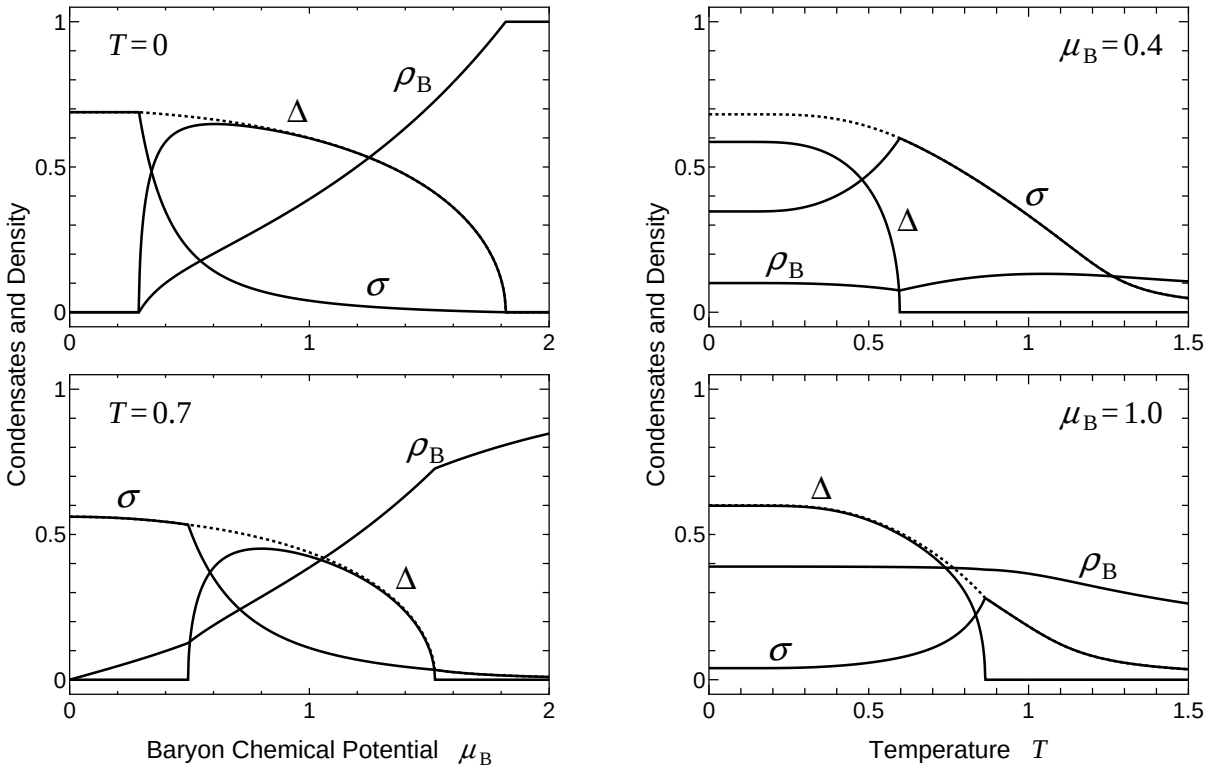

Figure 2: Chiral condensate σ, diquark condensate Δ, and baryon density ρ_B for $m = 0.02$ with $d = 3$. All the definitions are the same with those of Fig. 1 except that the dotted line indicates a total magnitude of the condensates $\sqrt{\sigma^2 + \Delta^2}$.

At $T = 0$ (the upper left panel), the diquark condensate Δ decreases monotonously as a function of μ_B and shows a second order transition when μ_B becomes of order unity. On the other hand, the baryon density ρ_B increases linearly for small μ_B and grows more rapidly for large μ_B until the saturation point where quarks occupy the maximally allowed configurations by the Fermi statistics. (See the analytical formula given in Eq. (49).) Those behaviors of Δ and ρ_B are also observed in the recent Monte-Carlo simulations of 2-color QCD [14]. Note that the rapid increase of ρ_B near the upper-critical chemical potential $\mu_c^{\rm up}$ takes place even in the strong coupling limit as shown here. Namely it does not necessarily be an indication of the existence of free quarks at high density unlike the suggestion given in the last reference in [14].

As T increases, the magnitude of the diquark condensate decreases by the thermal excitations of quark and anti-quark pairs in the last term of Eq. (40), which is shown in the lower left panel of Fig. 1. It is worth mentioning here that the diquark condensate disappears even before the complete saturation ($\rho_B = 1$) takes place.

Next we consider the diquark condensate as a functions of T for two typical values of the chemical potential in the right panels of Fig. 1. The diquark condensate shows a second order transition at T_c given analytically by Eq. (44).

3.4.2 Case for $m \neq 0$

In the upper left panel of Fig. 2, the chiral condensate, the diquark condensate and the baryon density are shown as functions of μ_B for small quark mass $m = 0.02$ at $T = 0$. As we have discussed in Sec. 3.3.2, there exists a lower-critical chemical potential $\mu_c^{\rm low}$ given by Eq. (55). Both Δ and ρ_B

start to take finite values only for $\mu_{\rm B} > \mu_{\rm c}^{\rm low}$ at $T = 0$.

One can view the behavior of chiral and diquark condensates with finite quark mass as the manifestation of two different mechanisms: One is a continuous "rotation" from the chiral direction to the diquark direction near $\mu_{\rm B} = \mu_{\rm c}^{\rm low}$ or $T = T_{\rm c}(\mu_{\rm B})$ with $\sqrt{\sigma^2 + \Delta^2}$ (shown by the dotted line) varying smoothly. The other is the saturation effect which forces the diquark condensate to decrease and disappear for large $\mu_{\rm B}$ as seen in the previous case of $m = 0$.

The "rotation" can be understood as follows: The free energy in the mean field approximation at small m and $\mu_{\rm B}$ has an approximate symmetry which mixes the chiral condensate with the diquark one as we have discussed in Sec. 3.3.1. The effect of m ($\mu_{\rm B}$) is to break this symmetry in the direction of the chiral (diquark) condensation favored. Therefore, a relatively large chiral condensate predominantly appears for small $\mu_{\rm B}$ region. (Note that the chiral symmetry is explicitly broken by m, thus the chiral condensate is always non-vanishing although it is suppressed in magnitude at high T and $\mu_{\rm B}$.) Just above the lower-critical chemical potential $\mu_{\rm c}^{\rm low}$, the chiral condensate decreases while the diquark condensate increases because the effect of $\mu_{\rm B}$ surpasses that of m. As $\mu_{\rm B}$ becomes large, the diquark condensate begins to decrease in turn by the effect of the saturation and eventually disappears when $\mu_{\rm B}$ exceeds the upper-critical value $\mu_{\rm c}^{\rm up}$ (order of unity for $T = 0$).

Similar "rotation" and the saturation effect are also seen at finite T as shown in the lower left panel of Fig. 2. At finite T, both the chiral and diquark condensates are suppressed due to the effect of temperature and the diquark condensate disappears before the complete saturation occurs.

Next we consider the chiral and diquark condensates as functions of T (the right panels of Fig. 2). At low T, both the chiral and diquark condensates have finite values for $\mu_{\rm B} = 0.4$ and 1.0. The diquark condensate decreases monotonously as T increases and shows a second order transition. On the other hand, the chiral condensate increases as the diquark condensate decreases so that the total condensate $\sqrt{\sigma^2 + \Delta^2}$ is a smoothly varying function of T. The understanding based on the chiral-diquark mixing symmetry is thus valid. An interesting observation is that the chiral condensate, although it is a continuous function of T, has a cusp shape associated with the phase transition of the diquark condensate.

Finally let us compare the $m = 0$ case in Fig. 1 and the $m = 0.02$ case in Fig. 2. Looking into two figures at the same temperature or chemical potential, we find that the diquark condensate Δ for $m = 0$ and the total condensate $\sqrt{\sigma^2 + \Delta^2}$ for $m = 0.02$ have almost the same behavior. This indicates that although the current quark mass suppresses the diquark condensate, the price to pay is to increase the chiral condensate so as to make the total condensate insensitive to the presence of small quark mass. Restating this by use of the radial and the angle variables defined by $\lambda \sin\phi = \sigma$ and $\lambda \cos\phi = |\Delta|$ as in Eq. (127), a small m hardly changes the behavior of λ but shifts ϕ from zero.

3.4.3 Phase diagrams

Now we show the phase diagram of the strong coupling 2-color QCD in the T-$\mu_{\rm B}$ plane in Fig. 3. The solid line denotes a critical line separating diquark superfluid phase $\Delta \neq 0$ and the normal phase $\Delta = 0$ in the chiral limit $m = 0$, which is determined analytically by Eq. (44). The dashed line denotes the critical line determined numerically for $m = 0.02$. The phase transition is of second order on these critical lines. The chiral condensate σ is everywhere zero for $m = 0$, while it is everywhere finite for $m \neq 0$. In the latter case, however, σ is particularly large in the region between the solid line and the dashed line. Shown in Fig. 4 is a phase diagram in $\mu_{\rm B}$-m plane at $T = 0$. The lower right of the figure corresponds to the vacuum with no baryon number present, $\rho_{\rm B} = 0$. On the other hand, the upper left of the figure corresponds to the saturated system, $\rho_{\rm B} = 1$, in which every lattice site is occupied by one baryon. There is a region with $0 < \rho_{\rm B} < 1$ and $\Delta \neq 0$ bounded by the above two limiting cases, which is separated by two critical lines given in Eq.(55).

It is worth mentioning here that we can see the corresponding system in the context of condensed matter physics; the hardcore boson Hubbard model has a similar phase diagram at $T = 0$ in which

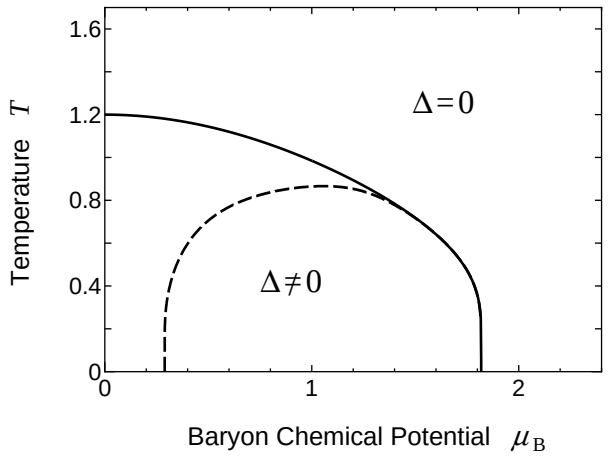

Figure 3: Phase diagram of the strong coupling 2-color QCD in the T-μ_B plane. Solid (dashed) line denotes the critical line for diquark condensation for $m = 0$ ($m = 0.02$).

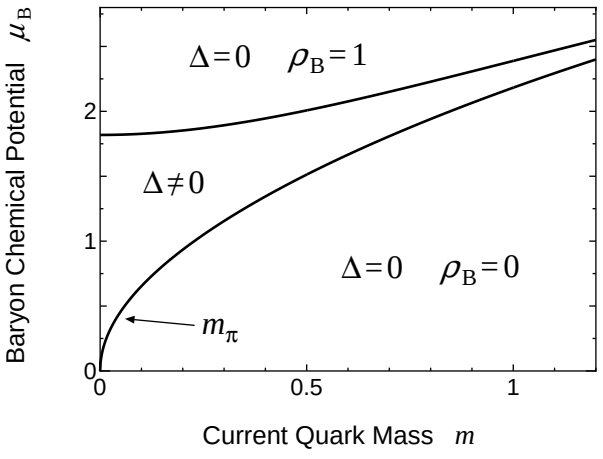

Figure 4: Phase diagram of strong coupling 2-color QCD in the μ_B-m plane at $T = 0$. Two solid lines separate the region where $\Delta = 0$ from the region where $\Delta \neq 0$.

superfluid phase is sandwiched by Mott-insulating phases with zero or full density [48]. Here we can give a physical explanation for the saturation effect, that is, why the saturated baryon density forces the diquark condensate to disappear. Suppose that one imposes the small external field for the baryon charge on the system in which every lattice site is occupied maximally by quarks. However, a diquark at one site cannot hop to the next site owing to the Pauli principle of constituent quarks and then the current for baryon charge never appears. It results in zero condensate because the superconducting current is proportional to the square of absolute value of the condensate. This is nothing but the analogical phenomenon with the Mott-insulator.

Finally, bringing all the discussions together, the phase structure in the three dimensional T-μ_B-m space is shown in Fig. 5. The diquark condensate has a none-vanishing value inside the critical surface and the phase transition is of second order everywhere on this critical surface. The second order phase transition is consistent with other analyses employing the mean field approximation; the random matrix model and the Nambu−Jona-Lasinio model [47] and also the chiral perturbation theory at $T = 0$ [36]. On the other hand, Monte-Carlo simulations of 2-color QCD [14] show indication of a tricritical point in the T-μ_B plane at which the property of the critical line changes from the second order to the first order as μ_B increases. This is also supported by the chiral perturbation theory beyond the mean field approximation at finite T [37].

Aside from the fact that we are working in the strong coupling limit ($g \to \infty$), though the lattice simulations are aiming at the weak coupling limit ($g \to 0$), it would be of great interests to go beyond the mean field approximation in our analysis and study corrections to the phase structure given in Fig. 5.

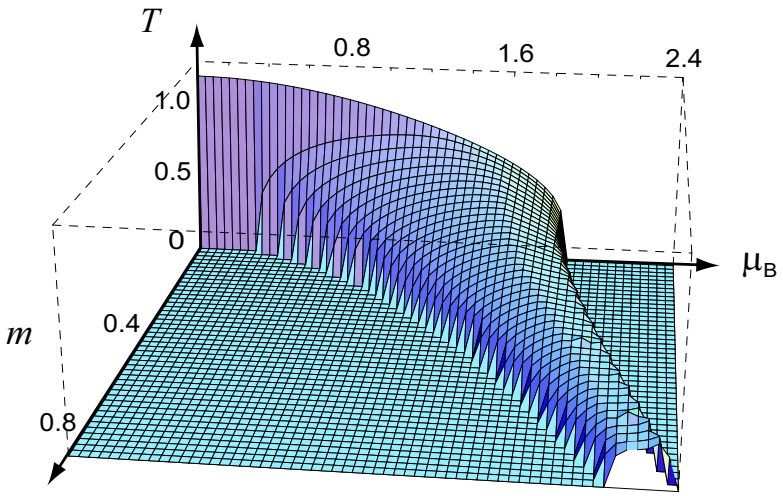

Figure 5: Phase structure of strong coupling 2-color QCD in the T-$\mu_{\rm B}$-m space. The surface represents the critical surface for the diquark condensation, which separates the region where $\Delta = 0$ from the region where $\Delta \neq 0$.

4 QCD ($N_{\rm c} \geq 3, N_{\rm f} = 4$) with finite baryon density

In this section, we consider the strong coupling lattice QCD with finite baryon density. First of all, we review how to derive the effective free energy written in terms of a scalar mode σ and a pseudoscalar mode π for $N_{\rm c} \geq 3$ for the further extension in Sec. 5, while the resultant free energy is almost same as that studied in [20, 21, 22]. Then we analyze the chiral phase transition in the chiral limit at finite temperature and density, and derive analytical formulae for second order critical line and tricritical point. Finally we show the phase diagram in terms of T and $\mu_{\rm B}$ for $N_{\rm c} = 3$.

4.1 Derivation of an effective action

4.1.1 Mean field approximation

In the staggered fermion formalism, one species of staggered fermion at various site is responsible for the degree of freedom of flavors and spins. Therefore the auxiliary field $\sigma(x)$ is responsible for both of the scalar mode σ and the pseudoscalar mode π [38]. In order to derive the effective action written by the scalar and pseudoscalar modes, we introduce σ and π as $\sigma(x) = \sigma + {\rm i}\varepsilon(x)\pi$ [39]. Then we can find a correspondence between these new values σ, π and vacuum expectation values of mesonic composites:

$$\sigma = -\frac{1}{N_{\rm c}} \langle \bar{\chi}^a(x)\chi^a(x) \rangle \ , \qquad \pi = \frac{1}{N_{\rm c}} \langle {\rm i}\, \bar{\chi}^a(x)\varepsilon(x)\chi^a(x) \rangle \ . \tag{59}$$

These equations tell us that the σ and π fields are even and odd under lattice parity respectively, where lattice parity is defined as [13, 40]

$$\chi(x) \mapsto \chi(x') \, , \quad \bar{\chi}(x) \mapsto \bar{\chi}(x') \, , \qquad x' = (x_0 + 1, -x_1, -x_2, -x_3) \, . \tag{60}$$

Therefore σ and π correspond to the spatially uniform condensates of scalar mode (chiral condensate) and pseudoscalar mode (pion condensate). They transform under ${\rm U(1)_A}$ transformation as

$${\rm U(1)_A} : \quad \begin{pmatrix} \sigma \\ \pi \end{pmatrix} \mapsto \begin{pmatrix} \cos 2\theta_{\rm A} & -\sin 2\theta_{\rm A} \\ \sin 2\theta_{\rm A} & \cos 2\theta_{\rm A} \end{pmatrix} \begin{pmatrix} \sigma \\ \pi \end{pmatrix} \ . \tag{61}$$

The partition function is then written as

$$Z = \int \mathcal{D}[U_0]\, \mathcal{D}[\chi, \bar{\chi}]\, \mathrm{e}^{-S'[U_0, \chi, \bar{\chi}; \sigma, \pi]}\,, \tag{62}$$

with

$$\begin{aligned} S'[U_0, \chi, \bar{\chi}; \sigma, \pi] = \sum_x \Bigg[& m\bar{\chi}(x)\chi(x) + \frac{1}{2}\left\{ \bar{\chi}(x)\mathrm{e}^{\mu} U_0(x)\chi(x+\hat{0}) - \bar{\chi}(x+\hat{0})\mathrm{e}^{-\mu} U_0^{\dagger}(x)\chi(x) \right\} \\ & + \frac{N_{\rm c} d}{4}\left(\sigma^2 + \pi^2\right) + \frac{N_{\rm c} d}{2}\left\{\sigma - \mathrm{i}\varepsilon(x)\pi\right\} M(x) \Bigg]\,. \end{aligned} \tag{63}$$

Note that this action contains hopping terms of χ, $\bar{\chi}$ only in the temporal direction after the $1/d$ expansion and the mean field approximation.

4.1.2 Integrations over χ, $\bar{\chi}$, and U_0

In order to complete the remaining integrals, we adopt the Polyakov gauge [20] in which $U_0(\tau, \vec{x})$ is diagonal and independent of τ;

$$U_0(\tau, \vec{x}) = \mathrm{diag}\left[\mathrm{e}^{\mathrm{i}\phi_1(\vec{x})/N_\tau}, \cdots, \mathrm{e}^{\mathrm{i}\phi_{N_{\rm c}}(\vec{x})/N_\tau}\right] \qquad \text{with} \quad \sum_{a=1}^{N_{\rm c}} \phi_a(\vec{x}) = 0\,. \tag{64}$$

Also we make a partial Fourier transformation for the quark fields;

$$\chi(\tau, \vec{x}) = \frac{1}{\sqrt{N_\tau}} \sum_{n=1}^{N_\tau} \mathrm{e}^{\mathrm{i}k_n\tau} \tilde{\chi}(n, \vec{x})\,, \quad \bar{\chi}(\tau, \vec{x}) = \frac{1}{\sqrt{N_\tau}} \sum_{n=1}^{N_\tau} \mathrm{e}^{-\mathrm{i}k_n\tau} \tilde{\bar{\chi}}(n, \vec{x})\,, \qquad k_n = 2\pi\frac{(n - \frac{1}{2})}{N_\tau}\,. \tag{65}$$

Substituting Eqs. (64) and (65) into the action (63) and taking the summation over τ, the Grassmann integration over the the quark fields χ and $\bar{\chi}$ results in the following determinant:

$$\prod_{\vec{x}} \prod_{a=1}^{N_{\rm c}} \prod_{n=1}^{N_\tau/2} \left[\sin^2 \bar{k}_n + M^2 + \left(\frac{d}{2}\pi\right)^2 \right] \tag{66}$$

with $\bar{k}_n = k_n + \phi_a(\vec{x})/N_\tau - \mathrm{i}\mu$. M denotes the dynamical quark mass defined by $M = m + (d/2)\sigma$.

The product with respect to the Matsubara frequencies n can be performed using a technique similar to that in the calculation of the free energy in finite temperature continuum field theory. The details of the calculation is given in Appendix A.2. The result turns out to be a quite simple form; $2\cosh\left[N_\tau E\right] + 2\cos\left[\phi_a(\vec{x}) - \mathrm{i}N_\tau\mu\right]$ with one-dimensional quark excitation energy $E[\sigma, \pi] = \mathrm{arcsinh}[\sqrt{M^2 + (d/2)^2\pi^2}]$.

Finally we can perform the integration with respect to U_0 by use of the formula in Appendix C for the Polyakov gauge. Then the integration gives, up to an irrelevant factor,

$$\int \mathcal{D}[U_0] \prod_{\vec{x}} \prod_{a=1}^{N_{\rm c}} \left\{ 2\cosh\left[N_\tau E\right] + 2\cos[\phi_a(\vec{x}) - \mathrm{i}N_\tau\mu] \right\} = \prod_{\vec{x}} \left\{ \sum_n \det_{i,j} P_{n+i-j} \right\}\,, \tag{67}$$

where

$$P_0 = 2\cosh\left[N_\tau E\right]\,, \qquad P_{\pm 1} = \cosh\left[N_\tau\mu\right] \pm \sinh\left[N_\tau\mu\right] = \mathrm{e}^{\pm N_\tau\mu} \qquad \text{and} \qquad P_{|n|\geq 3} = 0\,. \tag{68}$$

The determinant is to be taken with respect to $i, j = 1, 2, \cdots, N_{\rm c}$. The determinants have non-vanishing values only for $n = 0, \pm 1$ and the summation of them can be calculated exactly for general $N_{\rm c}$: Firstly for $n = 0$, $\det P_{i-j}$ is expressed by the form of $N_{\rm c} \times N_{\rm c}$ matrix as

$$\det_{i,j} P_{i-j} = \begin{vmatrix} P_0 & P_{-1} & 0 & \cdots \\ P_{+1} & P_0 & \ddots & \\ 0 & \ddots & \ddots & P_{-1} \\ \vdots & & P_{+1} & P_0 \end{vmatrix} . \tag{69}$$

Making the recursion formula for it and using the fact that $P_{-1}P_{+1} = 1$, we can obtain the simple solution as [20]

$$\det P_{i-j} = \frac{\sinh\left[(N_{\rm c}+1)N_\tau E\right]}{\sinh\left[N_\tau E\right]} . \tag{70}$$

Then the calculation for $n = \pm 1$ is rather easy and results in

$$\det P_{-1+i-j} + \det P_{1+i-j} = P_{-1}^{N_{\rm c}} + P_{+1}^{N_{\rm c}} = 2\cosh\left[N_{\rm c} N_\tau \mu\right] . \tag{71}$$

As a result, effective free energy is given as follows;

$$F_{\rm eff}[\sigma, \pi; T, \mu_{\rm B}] = (-\log Z) \,/\, (\textstyle\sum_x) = \frac{N_{\rm c} d}{4}\left(\sigma^2 + \pi^2\right) - T \log\left\{ 2\cosh\left[\mu_{\rm B}/T\right] + \frac{\sinh\left[(N_{\rm c}+1)E/T\right]}{\sinh\left[E/T\right]} \right\} . \tag{72}$$

Here we have defined the baryon chemical potential $\mu_{\rm B}$ as $\mu_{\rm B} = N_{\rm c}\mu$. This effective action corresponds to the 4 flavor QCD in the continuum limit. Hereafter we put $N_{\rm f} = 4$ and consider the effective free energy given in Eq. (72).

4.2 Analytical properties in the chiral limit

The effective free energy obtained in the previous subsection is simple enough to make analytical studies in the chiral limit. This is one of the main advantages of our approach. Such analytical studies on the chiral phase transition is useful to understand the phase structure of the strong coupling lattice QCD, which will be presented in the next subsection. In the chiral limit $m = 0$, the quark excitation energy reduces to $E[\sigma, \pi] = \mathrm{arcsinh}[(d/2)\sqrt{\sigma^2 + \pi^2}]$. Therefore the effective free energy in Eq.(72) is only a function of $\sqrt{\sigma^2 + \pi^2}$. Of course this symmetry comes from the chiral symmetry $\mathrm{U(1)_A}$ of the original lattice action. Since we can arbitrarily choose the direction of the condensate, we take $\sigma \neq 0$ and $\pi = 0$.

4.2.1 Chiral restoration at finite temperature

As we will confirm numerically in the next subsection, the effective free energy exhibits the second order phase transition at finite temperature. Therefore we can expand it in terms of the order parameter σ near the critical point. Expansion of effective free energy up to 2nd order of chiral condensate σ gives

$$F_{\rm eff}[\sigma, 0] = \frac{N_{\rm c} d}{4}\sigma^2 - \frac{d^2 N_{\rm c}(N_{\rm c}+1)(N_{\rm c}+2)}{24T(N_{\rm c} + 1 + 2\cosh\left[\mu_{\rm B}/T\right])}\sigma^2 + O\left(\sigma^4\right) . \tag{73}$$

As long as the coefficient of σ^4 is positive, the condition that the coefficient of σ^2 is zero gives critical chemical potential for the second order phase transition as a function of temperature;

$$\mu_{\rm B}^{\rm cri}(T) = T\,\mathrm{arccosh}\left[\frac{(N_{\rm c}+1)\{d(N_{\rm c}+2) - 6T\}}{12T}\right] . \tag{74}$$

The critical temperature at zero chemical potential is given by solving the equation $\mu_{\rm B}^{\rm cri}(T) = 0$ and turns out to be

$$T_{\rm c}(0) = \frac{d(N_{\rm c}+1)(N_{\rm c}+2)}{6(N_{\rm c}+3)}\,. \tag{75}$$

When the coefficient of σ^4 becomes zero, the phase transition becomes of first order. An analytical expression for the tricritical point $(T_{\rm tri}, \mu_{\rm tri})$ can be obtained as a solution of the coupled equations of Eq. (74) and $\partial^4 F_{\rm eff}/\partial\sigma^4 = 0$, and results in

$$T_{\rm tri} = \frac{\sqrt{225N_{\rm c}^2 + 20d^2(3N_{\rm c}^2+6N_{\rm c}-4)} - 15N_{\rm c}}{20d}\,, \quad \mu_{\rm tri} = \mu_{\rm B}^{\rm cri}(T_{\rm tri})\,. \tag{76}$$

The effective free energy exhibits the second order chiral phase transition for $T \geq T_{\rm tri}$ and it becomes of the first order for $T < T_{\rm tri}$. The existence of the tricritical point is consistent with results of other analytical approaches using Nambu−Jona-Lasinio model [26], random matrix model [27], Schwinger-Dyson equation [28] and other methods [29, 41, 42].

4.2.2 Chiral restoration at finite density

The analytical study of the first order chiral phase transition at finite temperature for $T < T_{\rm tri}$ is rather involved. However, the effective free energy reduces to a simpler form at $T = 0$;

$$F_{\rm eff}[T=0] = \frac{N_{\rm c}d}{4}\sigma^2 - \max\left\{\mu_{\rm B}, N_{\rm c}E[\sigma]\right\}\,, \quad E[\sigma] = \mathrm{arcsinh}\left[\frac{d}{2}\,|\sigma|\right]\,. \tag{77}$$

It is easy to study the first phase transition analytically in this case.

The effective free energy has two local minima as a function of σ: One is $F_{\rm eff} = -\mu_{\rm B}$ at $\sigma = 0$. The other is $F_{\rm eff} = N_{\rm c}d\,\sigma_0^2/4 - N_{\rm c}E[\sigma_0] < 0$ at $\sigma = \sigma_0$, where σ_0 is the solution of the chiral gap equation $\partial F_{\rm eff}/\partial\sigma = 0$;

$$\sigma_0^2\left[1 + \left(\frac{d}{2}\sigma_0\right)^2\right] = 1 \qquad \therefore \quad \sigma_0^2 = \frac{2\sqrt{1+d^2}-2}{d^2}\,. \tag{78}$$

As $\mu_{\rm B}$ becomes larger, the global minimum changes from $N_{\rm c}d\,\sigma_0^2/4 - N_{\rm c}E[\sigma_0]$ to $-\mu_{\rm B}$ at some value of the chemical potential. This is the critical chemical potential, given by

$$\mu_{\rm B}^{\rm cri}(T=0) = N_{\rm c}E[\sigma_0] - \frac{N_{\rm c}d}{4}\sigma_0^2\,. \tag{79}$$

At this critical point, the order parameter σ changes discontinuously as

$$\sigma(\mu) = \begin{cases} \sigma_0 & \text{when } \mu_{\rm B} < \mu_{\rm B}^{\rm cri}(T=0) \\ 0 & \text{when } \mu_{\rm B} > \mu_{\rm B}^{\rm cri}(T=0)\,. \end{cases} \tag{80}$$

This is the first order phase transition. Also we can easily calculate the baryon density $\rho_{\rm B}$ at $T = 0$ and it has discontinuity associated with that of the chiral condensate as

$$\rho_{\rm B} = -\frac{\partial F_{\rm eff}}{\partial\mu_{\rm B}} = \begin{cases} 0 & \text{when } \mu_{\rm B} < \mu_{\rm B}^{\rm cri}(T=0) \\ 1 & \text{when } \mu_{\rm B} > \mu_{\rm B}^{\rm cri}(T=0)\,. \end{cases} \tag{81}$$

At the critical chemical potential, $\rho_{\rm B}$ changes from the empty density 0 to the saturated density 1 [23]. Note that one baryon (= $N_{\rm c}$ quarks) at one lattice site, that is $\rho_{\rm B} = 1$, is the maximally allowed

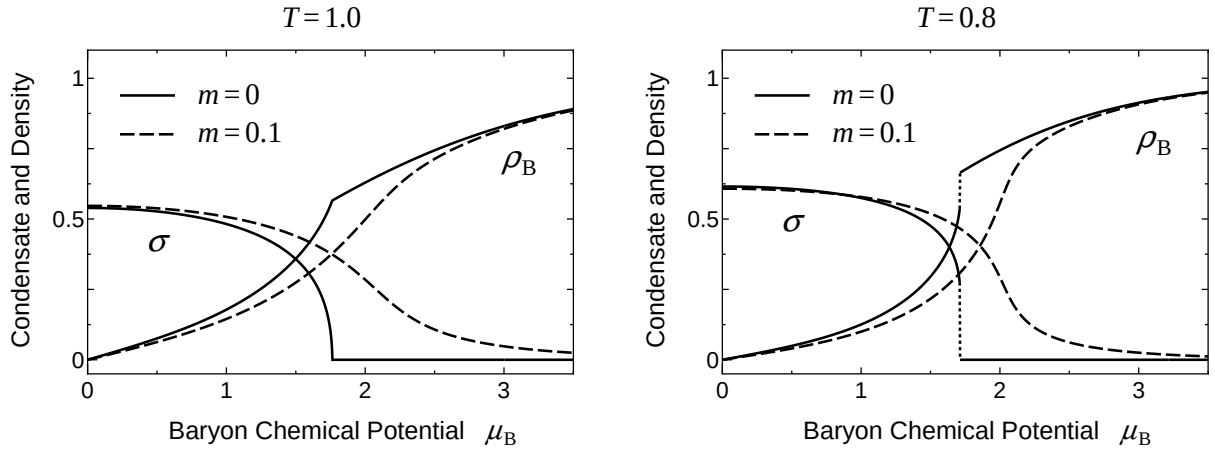

Figure 6: Chiral condensate σ and baryon density $\rho_{\rm B}$ as functions of the baryon chemical potential $\mu_{\rm B}$ for $N_{\rm c} = 3, N_{\rm f} = 4$. In the left panel, they are plotted just above the tricritical temperature ($T_{\rm tri} = 0.866$) at $T = 1.0$ for $m = 0$ (the solid line) and $m = 0.1$ (the dashed one). In the right panel, they are plotted just below $T_{\rm tri}$ at $T = 0.8$ for $m = 0$ (the solid line) and $m = 0.1$ (the dashed one).

configurations by the Fermi statistics for one species of staggered fermion. Such a saturation at large $\mu_{\rm B}$ on the lattice is already observed for $\mathrm{SU_c}(2)$ QCD in Sec. 3.

This chiral phase transition with finite $\mu_{\rm B}$ at $T = 0$ is not associated with the deconfinement phase transition to the quark matter, because we are in the strong coupling limit where quarks are always confined. Eqs. (80) and (81) show that the chiral restoration coincides with the transition from vacuum to the saturated nuclear matter, although they are in general separated [27]. Including the baryonic contribution, which is suppressed in the leading order $1/d$ expansion, will introduce the Fermi surface of baryons and hence make the two phase transitions separated.

4.3 The phase structure with finite quark mass

In this subsection, setting the number of colors and spatial dimensions to 3, we examine numerically the nature of the chiral phase transition and the phase diagram of strong coupling lattice QCD for $N_{\rm c} = 3, N_{\rm f} = 4$.

4.3.1 Chiral condensate and baryon density

By minimizing the effective free energy $F_{\rm eff}$ for $N_{\rm c} = 3$, $d = 3$ in terms of the order parameter σ, we determine the chiral condensate as a function of T and $\mu_{\rm B}$. The baryon density $\rho_{\rm B}$ is also calculated by $-\partial F_{\rm eff}/\partial \mu_{\rm B}$. In Fig. 6, the results with zero and finite m are shown as functions of $\mu_{\rm B}$.

In the left panel of Fig. 6, σ and $\mu_{\rm B}$ are shown for $T = 1.0$ just above $T_{\rm tri} = 0.866$. In the chiral limit they show second order phase transition at the critical chemical potential given by Eq. (74), while an infinitesimal introduction of m makes the transition smooth crossover.

σ and $\mu_{\rm B}$ are shown for $T = 0.8$ just below $T_{\rm tri}$ in the right panel of Fig. 6. As discussed in the previous subsection, they show jumps at the critical chemical potential in the chiral limit. This first order phase transition is weakened by the introduction of m and finally becomes a crossover for large quark masses.

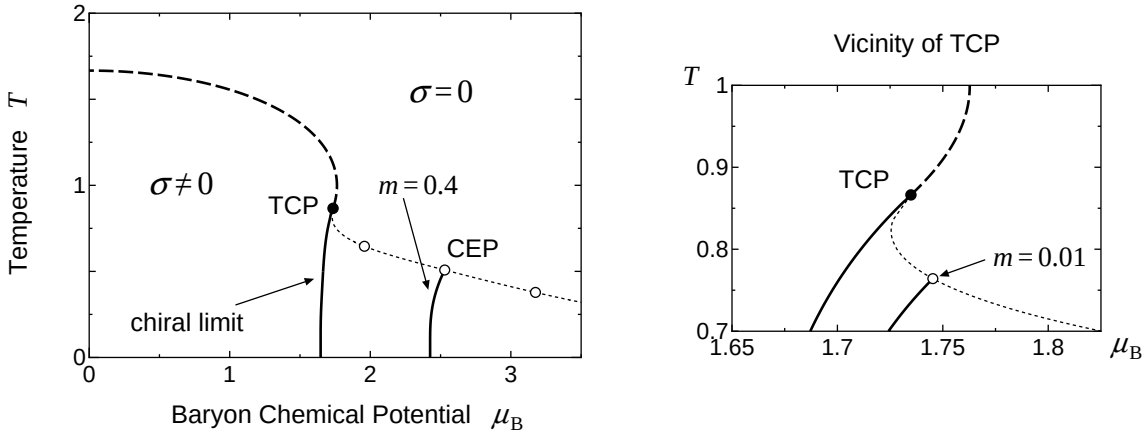

Figure 7: Phase diagram of strong coupling QCD with $N_c = 3, N_f = 4$ in the T-μ_B plane. The solid (dashed) line denotes the critical line for the first (second) order phase transition in the chiral limit. The black circle represents the tricritical point (TCP) where the nature of the phase transition changes from of the first order to the second. The first order line and its critical endpoint (CEP) for $m = 0.4$ are also shown. The dotted line denotes the flow of the critical endpoints when the quark mass is enlarged from 0. White circles are put on the critical endpoints for $m = 0.1$ (the left one), $m = 0.4$ (the middle) and $m = 0.8$ (the right one) in the left panel. The vicinity of TCP is zoomed up and the first order line and CEP for $m = 0.01$ are shown in the right panel.

4.3.2 The phase diagram

Now we show in Fig. 7 the phase diagram of the strong coupling lattice QCD with $N_c = 3, N_f = 4$ in the plane of T and μ_B. In the chiral limit, chiral condensate σ has non-vanishing value at low T and small μ_B, which means spontaneous breakdown the the chiral symmetry $U_A(1)$ by the condensation $\sigma \neq 0$. The symmetry broken phase is separated by phase transition from chiral symmetric phase; the phase transition is of second order in the high temperature region while it is of first order in the low temperature region. The second order critical line merges smoothly into the first order one at the tricritical point $(T_{tri}, \mu_{tri}) = (0.866, 1.73)$.

In contradiction to our result, the chiral phase transition of 4 flavor QCD in the chiral limit is thought to be of first order [9, 12]. This difference comes from the fact that we have employed the mean field approximation and ignored the chiral fluctuations. However, it is sensible to consider that the second order critical line in our result is accountable for the critical line of chiral restoration in QCD.

As we can find from Fig. 7, the critical temperature falls much rapidly as a function of μ_B in contrast to the results from recent Monte-Carlo simulations at small chemical potential [9, 10, 11, 12]. In order to make the discussion quantitative, we calculate the slope of the critical temperature near zero chemical potential. From Eq. (74):

$$\frac{T_c(\mu)}{T_c(0)} = 1 - 1.5\frac{\mu^2}{T_c(0)^2} - 3.375\frac{\mu^4}{T_c(0)^4} + O\left((\mu/T_c)^6\right) \tag{82}$$

with $T_c(0) = 5/3$. Here we have written Eq. (82) in terms of the quark chemical potential $\mu = \mu_B/N_c$ in order to make the comparison to the lattice data easy. The values of the coefficient of the 2nd term is two orders of magnitude larger than that calculated in the lattice simulation with $N_f = 4$ for $m = 0.05$ [12]. This large difference in the slope of chiral phase transition may be understood due to the effect of $m = 0$ and that of $g \to \infty$. Our expression (82) is derived in the chiral limit, while all of the lattice simulations are performed with finite quark mass. As reported in [43], the chiral phase

Table 2: Tricritical point $(T_{\rm tri}, \mu_{\rm tri})$ for $m = 0$ and critical endpoints $(T_{\rm end}, \mu_{\rm end})$ for various small quark masses. The percentages of how far the critical endpoints are from the tricritical point are also shown.

m	$T_{\rm end}$	$\mu_{\rm end}$	$(T_{\rm end} - T_{\rm tri})/T_{\rm tri}$	$(\mu_{\rm end} - \mu_{\rm tri})/\mu_{\rm tri}$
0	0.866	1.73	—	—
0.001	0.823	1.73	−5.03 %	−0.541 %
0.01	0.764	1.75	−11.8 %	0.599 %
0.05	0.690	1.85	−20.4 %	6.37 %
0.1	0.646	1.96	−25.5 %	12.9 %
0.2	0.590	2.16	−31.9 %	24.7 %

transition line has significant quark mass dependence in the lattice simulations: The slope of $T_{\rm c}(\mu)$ suffers sharp increase by decreasing m, from 0.025 ($m = 0.1$) to 0.114 ($m = 0.005$) in $N_{\rm f} = 3$ QCD. In addition to that, as we can find in [22], the introduction of the next to leading order term of $1/g^2$ and $1/d$ to the strong coupling lattice QCD decreases the critical temperature and the amount of decrease at zero chemical potential is more than that at finite chemical potential. Therefore the slope of the critical temperature will be softer by the corrections for the strong coupling and large dimensional expansions. Combining the above two effects, the difference of the slope between our result and lattice simulations could become reasonably small, which needs further study.

Next we consider the effect of quark mass on the phase diagram. Introduction of finite m washes out the second order phase transition as shown in left panels of Fig. 6. As a result, the first order critical line terminates at second order critical endpoint $(T_{\rm end}, \mu_{\rm end})$. As long as the quark mass is very small $m \lesssim 0.001$, the critical endpoint flows almost along the tangent line at tricritical point as in the right panel of Fig. 7. Then for the larger quark mass $m \gtrsim 0.001$, $T_{\rm end}$ decreases and $\mu_{\rm end}$ increases. Also, the first order critical line shifts in the direction of large $\mu_{\rm B}$ associated with this change.

The strong coupling lattice QCD may give us some indication for lattice simulations about the effect of m on the phase diagram of QCD. As shown in Table 2, finite quark mass $m = 0.1$ decreases $T_{\rm end}$ by 25% and increases $\mu_{\rm end}$ by 12% from tricritical point $(T_{\rm tri}, \mu_{\rm tri})$. We can find in the same way that even a quark mass as small as $m = 0.001$ can move the critical endpoint by 5%. This indicates the relatively large dependence of the phase diagram of QCD on the quark mass.

Our phase structure is consistent with those from other analytical approaches [26, 27, 28, 29, 41, 42], except for one main difference [25]. It is the fact that $\mu_{\rm tri}$ or $\mu_{\rm end}$ is larger than the critical chemical potential at $T = 0$ for every quark mass and then the gradient of critical line near the tricritical point or critical endpoint is positive. In addition, critical endpoint flows in the direction of smaller T and smaller $\mu_{\rm B}$ as a function of quark mass $m \leq 0.001$. Such properties near the tricritical point conflict with the assumption made in [42] that the gradient of critical line near the tricritical point is negative. While this feature is not easy to interpret from physical point of view, such new possibility in the phase structure should be studied more.

5 QCD ($N_{\rm c} \geq 3, N_{\rm f} = 8$) with finite isospin density

In this section, we consider the strong coupling lattice QCD with finite isospin density. First of all, we derive the analytical expression for the effective free energy in two particular cases: One is at finite T, finite $\mu_{\rm B}$ and *small* $\mu_{\rm I}$ with the chiral condensates. The other is at finite T, finite $\mu_{\rm I}$ and *zero* $\mu_{\rm B}$ with the chiral and pion condensates. Then we analyze the effective free energy and show the phase diagrams in terms of T and $\mu_{\rm B}$ or $\mu_{\rm I}$ for $N_{\rm c} = 3, N_{\rm f} = 8$.

5.1 Strong coupling lattice QCD with isospin chemical potential

In order to investigate the effect of the isospin chemical potential $\mu_{\rm I}$ on the phase structure of QCD, we have to extend the lattice action studied in the previous section to that with two species of staggered fermion having degenerate masses. The lattice action with two species of staggered fermion corresponds to the 8 flavor QCD in the continuum limit. Then for $m = 0$ and $\mu_{\rm I} = 0$, it has $\mathrm{U(2)_V \times U(2)_A}$ symmetry, as a remnant of 8 flavor chiral symmetry, defined by

$$\chi(x) \mapsto \mathrm{e}^{\mathrm{i}(\theta_{\rm V} + \varepsilon(x)\theta_{\rm A})\cdot\tau}\chi(x) \qquad \text{and} \qquad \bar{\chi}(x) \mapsto \bar{\chi}(x)\mathrm{e}^{-\mathrm{i}(\theta_{\rm V} - \varepsilon(x)\theta_{\rm A})\cdot\tau} \tag{83}$$

with $\tau \in \mathrm{U(2)}$.

After integrating out the spatial link variable U_j in the leading order of $1/d$ expansion and introducing the auxiliary fields, we have the following partition function;

$$Z = \int \mathcal{D}[U_0]\,\mathcal{D}[\chi,\bar{\chi}]\,\mathcal{D}[\sigma]\,\mathrm{e}^{-S'[U_0,\chi,\bar{\chi};\sigma]}\,, \tag{84}$$

with

$$\begin{aligned} S'[U_0,\chi,\bar{\chi};\sigma] = &\sum_{\alpha={\rm u,d}}\sum_{x,y}\bar{\chi}_\alpha(x)\left[m\delta_{x,y} + \frac{1}{2}\left\{\mathrm{e}^{\mu_\alpha}U_0(x)\delta_{y,x+\hat{0}} - \mathrm{e}^{-\mu_\alpha}U_0^\dagger(x)\delta_{y,x-\hat{0}}\right\}\right]\chi_\alpha(y) \\ &+ \sum_{x,y}\left[\sigma_{\beta\alpha}(x)V_{\rm M}(x,y)\sigma_{\alpha\beta}(y) + 2\sigma_{\beta\alpha}(x)V_{\rm M}(x,y)M_{\alpha\beta}(y)\right]\,. \end{aligned} \tag{85}$$

Here the subscripts α, β represent the species of staggered fermion taking "u" (up quark) and "d" (down quark). $\mu_{\rm u}$, $\mu_{\rm u}$ are quark chemical potentials for each species of staggered fermion. $\sigma_{\alpha\beta}(x)$ are auxiliary fields for the mesonic composites $M_{\alpha\beta}(x) = \bar{\chi}^a_\alpha(x)\chi^a_\beta(x)/N_{\rm c}$, and these vacuum expectation values read $\langle\sigma_{\alpha\beta}(x)\rangle = -\langle M_{\alpha\beta}(x)\rangle$.

Now we replace the auxiliary fields $\sigma_{\rm uu}(x)$ and $\sigma_{\rm dd}(x)$ by the spatially uniform condensates of scalar mode as

$$\sigma_{\rm uu}(x) = \sigma_{\rm u}\,, \qquad \sigma_{\rm dd}(x) = \sigma_{\rm d}\,. \tag{86}$$

Then we find that $\sigma_{\rm u}$ and $\sigma_{\rm d}$ correspond to the chiral condensates of up and down quarks:

$$\sigma_{\rm u} = -\frac{1}{N_{\rm c}}\left\langle\bar{\rm u}^a(x){\rm u}^a(x)\right\rangle \qquad \text{and} \qquad \sigma_{\rm d} = -\frac{1}{N_{\rm c}}\left\langle\bar{\rm d}^a(x){\rm d}^a(x)\right\rangle\,. \tag{87}$$

Also we replace $\sigma_{\rm ud}(x)$ and $\sigma_{\rm du}(x)$ by the spatially uniform condensates of pseudoscalar mode as

$$\sigma_{\rm ud}(x) = \mathrm{i}\varepsilon(x)\pi\,, \qquad \sigma_{\rm du}(x) = \mathrm{i}\varepsilon(x)\pi^*\,. \tag{88}$$

Then π corresponds to the charged pion condensates:

$$\pi = \frac{1}{N_{\rm c}}\left\langle\mathrm{i}\,\bar{\rm u}^a(x)\varepsilon(x){\rm d}^a(x)\right\rangle \qquad \text{and} \qquad \pi^* = \frac{1}{N_{\rm c}}\left\langle\mathrm{i}\,\bar{\rm d}^a(x)\varepsilon(x){\rm u}^a(x)\right\rangle\,. \tag{89}$$

Substituting these mean field values and Eqs. (64), (65) to the action (85), we obtain

$$S'[\phi,\chi,\bar{\chi};\sigma_{\rm u},\sigma_{\rm d},\pi] = \sum_x \frac{N_{\rm c}d}{4}\left(\sigma_{\rm u}^2+\sigma_{\rm d}^2+2\left|\pi\right|^2\right) - \sum_{\vec{x}}\sum_a\sum_{m,n}\bar{X}(m,\vec{x})\,G^{-1}(m,n;\vec{x},\phi_a)\,X(n,\vec{x})\,, \tag{90}$$

where

$$\bar{X}(m,\vec{x}) = \left(\bar{\tilde{\rm u}}(m,\vec{x}),\bar{\tilde{\rm d}}(m,\vec{x})\right) \qquad \text{and} \qquad X(n,\vec{x}) = \begin{pmatrix}\tilde{\rm u}(n,\vec{x})\\ \tilde{\rm d}(n,\vec{x})\end{pmatrix}, \tag{91}$$

and

$$G^{-1}(m,n;\vec{x},\phi_a) \tag{92}$$
$$= \begin{pmatrix} -\left[M_{\rm u}+{\rm i}\sin\left(k_m+\dfrac{\phi_a(\vec{x})}{N_\tau}-{\rm i}\mu_{\rm u}\right)\right]\delta_{mn} & {\rm i}\varepsilon(\vec{x})\dfrac{d}{2}\pi^*\delta_{n,m-N_\tau/2} \\ {\rm i}\varepsilon(\vec{x})\dfrac{d}{2}\pi\delta_{n,m-N_\tau/2} & -\left[M_{\rm d}+{\rm i}\sin\left(k_m+\dfrac{\phi_a(\vec{x})}{N_\tau}-{\rm i}\mu_{\rm d}\right)\right]\delta_{mn}\end{pmatrix}.$$

$M_{\rm u} = m+(d/2)\sigma_{\rm u}$ and $M_{\rm d} = m+(d/2)\sigma_{\rm d}$ are dynamical quark masses of up and down quarks. After performing the integration over the Grassmann variables X and $\bar{X}$, we obtain the following effective free energy;

$$F_{\rm eff}[\sigma_{\rm u},\sigma_{\rm d},\pi;T,\mu_{\rm B},\mu_{\rm I}] = \frac{N_{\rm c}d}{4}\left(\sigma_{\rm u}^2+\sigma_{\rm d}^2+2\left|\pi\right|^2\right) - T\log\left\{\int {\rm d}U_0\prod_{a=1}^{N_{\rm c}}{\rm Det}\left[G^{-1}(\phi_a)\right]\right\}, \tag{93}$$

where

$${\rm Det}\left[G^{-1}(m,n;\vec{x},\phi_a)\right] = \prod_{n=1}^{N_\tau}\left[\left(\frac{d}{2}\right)^2\left|\pi\right|^2+\left\{M_{\rm u}+{\rm i}\sin\left(\bar{k}_n-{\rm i}\mu_{\rm I}\right)\right\}\cdot\left\{M_{\rm d}-{\rm i}\sin\left(\bar{k}_n+{\rm i}\mu_{\rm I}\right)\right\}\right] \tag{94}$$

with $\bar{k}_n = k_n+\phi_a(\vec{x})/N_\tau-{\rm i}\mu_{\rm B}/N_{\rm c}$: Here we have rewritten the chemical potentials of up and down quarks by $\mu_{\rm B}$ and $\mu_{\rm I}$ using the definition

$$\mu_{\rm u} = \frac{\mu_{\rm B}}{N_{\rm c}}+\frac{\mu_{\rm I}}{2} \qquad \text{and} \qquad \mu_{\rm d} = \frac{\mu_{\rm B}}{N_{\rm c}}-\frac{\mu_{\rm I}}{2}\,. \tag{95}$$

The integration over U_0 in Eq. (93) is defined in Appendix C.

It is impossible to perform the summation over n in Eq. (94) analytically for general $\mu_{\rm B}$ and $\mu_{\rm I}$. However, we can do in two interesting cases: One is the case that $\mu_{\rm I}$ is lower than a critical value $\mu_{\rm I}^{\rm cri}\sim m_\pi$, where the pion does not condensate $\pi=0$ [15]. This case is relevant to the realistic systems such as heavy ion collisions and electro-neutral neutron stars. The other is the case that $\mu_{\rm B}=0$, which means we can put $\sigma_{\rm u}=\sigma_{\rm d}$. In this case, we can compare our results with those obtained by the recent Monte-Carlo lattice simulations [16].

5.2 The phase structure for $\mu_{\rm I} < m_\pi$

First, we derive the analytical expression for the effective free energy in the case of $\mu_{\rm I} < \mu_{\rm I}^{\rm cri}$, where we can put $\pi=0$. The proof for the existence of such a critical value and its correspondence to the pion mass in the framework of strong coupling lattice QCD will be given in the next subsection. In this case, we can calculate the product over n using the formula in Appendix A.2;

$$\begin{aligned}&{\rm Det}\left[G^{-1}(m,n;\vec{x},\phi_a)\right]\\ &= \prod_{n=1}^{N_\tau}\left\{M_{\rm u}+{\rm i}\sin\left(k_n+\phi_a(\vec{x})/N_\tau-{\rm i}\mu_{\rm u}\right)\right\}\cdot\left\{M_{\rm d}+{\rm i}\sin\left(k_n+\phi_a(\vec{x})/N_\tau-{\rm i}\mu_{\rm d}\right)\right\}\\ &= \left\{2\cosh\left[N_\tau E_{\rm u}\right]+2\cos[\phi_a(\vec{x})-{\rm i}N_\tau\mu_{\rm u}]\right\}\cdot\left\{2\cosh\left[N_\tau E_{\rm d}\right]+2\cos[\phi_a(\vec{x})-{\rm i}N_\tau\mu_{\rm d}]\right\}\end{aligned} \tag{96}$$

with one-dimensional up and down quark excitation energy $E_u = \mathrm{arcsinh} M_u$, $E_d = \mathrm{arcsinh} M_d$.

Using the formula in Appendix C, we can complete the SU(N_c) integration over U_0 in Eq. (93) for general N_c. Then we obtain the analytical expression for the effective free energy as follows;

$$F_{\rm eff}[\sigma_u, \sigma_d; T, \mu_B, \mu_I < \mu_I^{\rm cri}] = \frac{N_c d}{4}\left(\sigma_u^2 + \sigma_d^2\right) - T \log\left\{\sum_n \det_{i,j} Q_{n+i-j}\right\}, \tag{97}$$

where

$$\begin{aligned} Q_0 &= 4\cosh\left[E_u/T\right]\cdot\cosh\left[E_d/T\right] + 2\cosh\left[(\mu_u - \mu_d)/T\right], \\ Q_{\pm 1} &= 2\cosh\left[E_u/T\right]\cdot\left(\cosh\left[\mu_d/T\right] \pm \sinh\left[\mu_d/T\right]\right) + 2\cosh\left[E_d/T\right]\cdot\left(\cosh\left[\mu_u/T\right] \pm \sinh\left[\mu_u/T\right]\right), \\ Q_{\pm 2} &= \cosh\left[(\mu_u + \mu_d)/T\right] \pm \sinh\left[(\mu_u + \mu_d)/T\right], \qquad Q_{|n|\geq 3} = 0 \end{aligned} \tag{98}$$

and the determinant is to be taken with respect to $i, j = 1, 2, \cdots, N_c$.

Although the effective free energy has the very complicated expression, it reduces to a simple form for $\mu_I = 0$ and $T = 0$. At $\mu = \mu_u = \mu_d$, we can put $\sigma = \sigma_u = \sigma_d$. Additionally in the zero temperature limit,

$$Q_0 \simeq \mathrm{e}^{2E/T}, \qquad Q_{+1} \simeq \mathrm{e}^{(E+\mu)/T}, \qquad Q_{+2} \simeq \mathrm{e}^{2\mu/T}, \qquad Q_{-1} \simeq Q_{-2} \simeq 0. \tag{99}$$

When $E > \mu$, Q_0 gives the dominant contribution to the effective free energy. On the other hand, when $\mu > E$, Q_{+2} gives the dominant contribution. Therefore we can write the effective free energy for $\mu_I = 0$ and $T = 0$ in terms of $\mu_B = N_c\mu$ as follows;

$$F_{\rm eff}[\sigma; T = 0, \mu_B, \mu_I = 0] = 2\left[\frac{N_c d}{4}\sigma^2 - \max\left\{\mu_B, N_c E[\sigma]\right\}\right]. \tag{100}$$

This expression coincides with the effective free energy at $T = 0$ (77) studied in the previous section up to the factor 2, which comes from the fact that we are now studying with "two" species of staggered fermion. Therefore the discussions on chiral restoration at finite density given in Sec. 4.2 hold true here by replacing the maximally allowed baryon density with $\rho_B = 2$.

5.2.1 The phase diagrams

At finite temperature, the integration over the temporal gauge link variable ϕ_a of Eq. (96) non-trivially couples the up and down quark sectors. Let us see its consequences numerically here. We show in Fig. 8 the phase diagram in the plane of T and μ_B with $N_f = 8$, determined by minimizing the effective free energy Eq. (97) for $N_c = 3$, $d = 3$ with respect to the order parameters σ_u, σ_d.

First we consider the case of $\mu_I = 0$ in which we can put $\sigma_u = \sigma_d$, and the phase diagram is shown in the left panel of Fig. 8. This should be compared to the case of 4 flavor QCD in Fig. 7. The outline of phase diagrams is quite consistent and the discussions given in Sec. 4.3 hold true here, while the critical temperature for $N_f = 8$ flavor is lower than that for $N_f = 4$. This is expected from physical point view: With more flavors, the chiral condensate is faster broken by their thermal excitations. In other words, the critical temperature decreases by increasing the number of quark flavors.

Next we consider the phase diagram at $\mu_I = 0.2$ with $m = 0.4$. As shown in the right panel of Fig. 8, the introduction of μ_I splits the first order phase transition line to the lines associated with the jump of chiral condensate of up quark and that of down quark. They shift in the opposite directions of μ_B and terminate at the second order critical endpoints. Such a successive chiral restoration with finite μ_I as increasing μ_B is easy to understand intuitively from the fact that up and down quarks suffer the chemical potential differently, $\mu_u = \mu_B/N_c + \mu_I/2$ and $\mu_d = \mu/N_c - \mu_I/2$.

What is non-trivial in our result is the position of the critical endpoints. The temperatures of critical endpoints for σ_u and σ_d are both higher than that in the case of $\mu_I = 0$. This is in contrast to

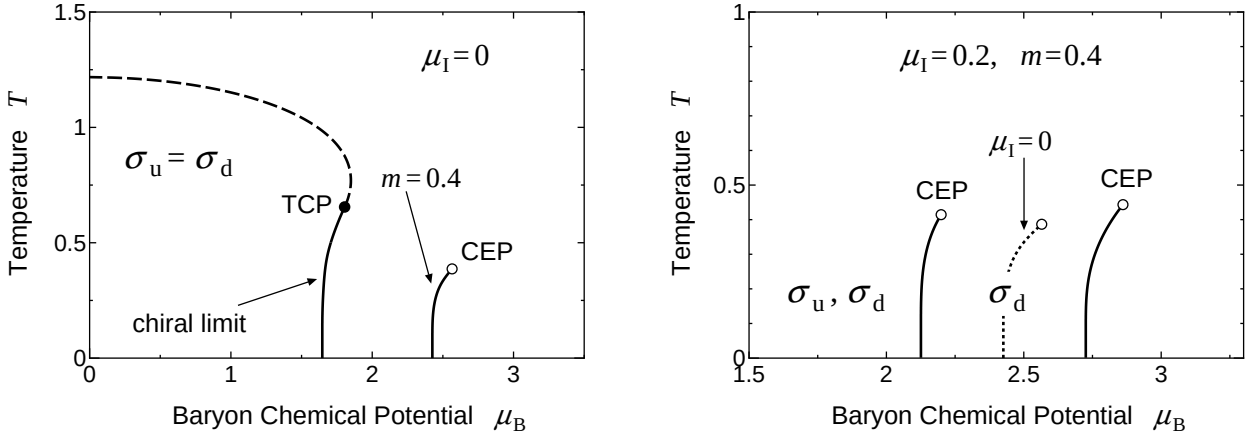

Figure 8: Phase diagrams of strong coupling QCD with $N_{\rm c} = 3, N_{\rm f} = 8$ in the T-$\mu_{\rm B}$ plane with zero (the left panel) and finite (the right one) isospin chemical potential $\mu_{\rm I}$. In the left panel, the solid (dashed) line denotes the critical line for the first (second) order phase transition in the chiral limit at $\mu_{\rm I} = 0$. The first order line and its critical endpoint for $m = 0.4$ are also shown. The right panel shows the phase diagram at $\mu_{\rm I} = 0.2$ and $m = 0.4$. Two solid lines represent the critical lines for the first order phase transitions associated with up (the left line) and down (the right one) quark condensates respectively. The first order phase transition line for $\mu_{\rm I} = 0$ is plotted by dotted line for comparison. The symbol $\sigma_{\rm u}$ or $\sigma_{\rm d}$ in the figure represents the region where the condensate has large value.

the study using random matrix model [44], Nambu−Jona-Lasinio model [45] and ladder-QCD approach [46], where the temperature of critical endpoints are not affected by $\mu_{\rm I}$ because up quark sector and down quark sector are completely uncoupled in such approaches. In our approach, as discussed above, up and down quarks are non-trivially coupled via the integration of the temporal gauge link variable U_0 at finite temperature.

5.3 The phase structure for $\mu_{\rm B} = 0$

We derive the analytical expression for the effective free energy in the case of $\mu_{\rm B} = 0$. In this case, we can put $\sigma = \sigma_{\rm u} = \sigma_{\rm d}$ and obtain the following expression for Eq. (94);

$$\begin{aligned}&\mathrm{Det}\left[G^{-1}(m,n;\vec{x},\phi_a)\right] \\ &= \prod_{n=1}^{N_\tau}\left[\left(\frac{d}{2}\right)^2|\pi|^2 + \left\{M + \mathrm{i}\sin\left(k_n + \frac{\phi_a(\vec{x})}{N_\tau} - \mathrm{i}\frac{\mu_{\rm I}}{2}\right)\right\}\cdot\left\{M - \mathrm{i}\sin\left(k_n + \frac{\phi_a(\vec{x})}{N_\tau} + \mathrm{i}\frac{\mu_{\rm I}}{2}\right)\right\}\right].\end{aligned} \tag{101}$$

This expression has the same form as the determinant calculated in Sec. 3.2 for $\mathrm{SU_c}(2)$ QCD. Therefore we can use the formula in Appendix A.1 for the product over the Matsubara frequencies, and then we obtain

$$\mathrm{Det}\left[G^{-1}(m,n;\vec{x},\phi_a)\right] = \{2\cosh\left[N_\tau E_-\right] + 2\cos\left[\phi_a(\vec{x})\right]\}\cdot\{2\cosh\left[N_\tau E_+\right] + 2\cos\left[\phi_a(\vec{x})\right]\} \tag{102}$$

with one-dimensional up quark and down anti-quark (or up anti-quark and down quark) excitation energy

$$E_\pm = \mathrm{arccosh}\left(\sqrt{(1+M^2)\cosh^2\left[\mu_{\rm I}/2\right] + (d/2)^2|\pi|^2} \pm M\sinh\left[\mu_{\rm I}/2\right]\right). \tag{103}$$

Using the formula in Appendix C, we can complete the SU(N_c) integration over U_0 in Eq. (93) for general N_c. Then we obtain the analytical expression for the effective free energy as follows;

$$F_{\rm eff}[\sigma,\pi;T,\mu_B=0,\mu_I] = \frac{N_c d}{2}\left(\sigma^2+|\pi|^2\right) - T\log\left\{\sum_n \det_{i,j} R_{n+i-j}\right\}, \tag{104}$$

where

$$\begin{aligned} R_0 &= 4\cosh\left[E_-/T\right]\cdot\cosh\left[E_+/T\right]+2\,, \\ R_{\pm1} &= 2\cosh\left[E_-/T\right]+2\cosh\left[E_+/T\right]\,, \\ R_{\pm2} &= 1\,, \qquad R_{|n|\geq 3}=0 \end{aligned} \tag{105}$$

and the determinant is to be taken with respect to $i,j=1,2,\cdots,N_c$. Note that for $m=0$ and $\mu_I=0$, the effective free energy is a function only in terms of $\sigma^2+|\pi|^2$. Of course this is from the chiral symmetry $U(2)_A$ of the original action at $m=\mu_I=0$. The symmetry between σ and π will play an important role in understanding numerical results on the phase structure.

Although the effective free energy has the very complicated expression, it reduces to a simple form at $T=0$. In the zero temperature limit,

$$R_0 \simeq {\rm e}^{(E_-+E_+)/T} \gg R_{\pm1} \simeq {\rm e}^{\max\{E_-,E_+\}/T} \gg R_{\pm2}\,, \tag{106}$$

because E_- and E_+ are positive. Therefore we can neglect the contribution of $R_{\pm1}, R_{\pm2}$ in Eq. (104), and then we obtain the effective free energy for $\mu_B=0$ and $T=0$ as follows;

$$F_{\rm eff}[\sigma,\pi;T=0,\mu_B=0,\mu_I] = \frac{N_c d}{2}\left(\sigma^2+|\pi|^2\right) - T\log\left\{R_0^{N_c}\right\} = N_c\left[\frac{d}{2}\left(\sigma^2+|\pi|^2\right)-(E_-+E_+)\right]. \tag{107}$$

If we replace π by Δ and μ_I by μ_B, the above expression corresponds to the free energy at $T=0$ of $SU_c(2)$ QCD studied in Sec. 3 up to the overall factor N_c. This correspondence is rather natural from the point of view of the symmetry and the effect of chemical potential. In the present system, up and down quarks are indistinguishable because of chiral symmetry at $\mu_I=0$ and they undergo the effect of μ_I with opposite signs. On the other hand in $SU_c(2)$ QCD, quark and anti-quark are indistinguishable because of the Pauli-Gürsey symmetry [33] at $\mu=0$ and they also undergo the effect of μ_B with opposite signs. Therefore there is a correspondence between up (down) quark in the finite isospin density system and (anti-) quark in the finite baryon density $SU_c(2)$ system, which also means the correspondence between the pion condensation and the diquark condensation. Note that the difference of the effective free energy in the two systems at $T\neq 0$ is due to the integration of U_0 for the finite isospin density system which couples up and down quarks non-trivially at finite temperature.

As calculated in Sec. 3.3 for the case of $SU_c(2)$ QCD, we can derive analytical properties from the effective free energy at $T=0$ in Eq. (107). The system has two critical chemical potentials, the lower one $\mu_c^{\rm low}$ and the upper one $\mu_c^{\rm up}$ given respectively by

$$\mu_c^{\rm low} = 2\,{\rm arccosh}\sqrt{1+mM} \quad \text{and} \quad \mu_c^{\rm up} = 2\,{\rm arccosh}\sqrt{1+K^2}\,, \tag{108}$$

where M is a solution of the chiral gap equation with quark mass m, and K is defined as the solution of Eq. (56). The non-vanishing value of pion condensate $\pi\neq 0$ is possible only for $\mu_c^{\rm low}\leq\mu_I\leq\mu_c^{\rm up}$. As long as $\mu_I<\mu_c^{\rm low}$, the empty vacuum gives $\rho_I=-\partial F_{\rm eff}/\partial\mu_I=0$ and $\pi=0$. On the other hand, for $\mu_I>\mu_c^{\rm up}$, the saturation of the isospin density occurs leading to $\rho_I=N_c$ and $\pi=0$. For sufficiently small m, the lower critical chemical potential reduces to

$$\mu_c^{\rm low} = 2\,m^{1/2}\cdot\left\{\frac{(1+d^2)^{1/2}-1}{2}\right\}^{1/4}. \tag{109}$$

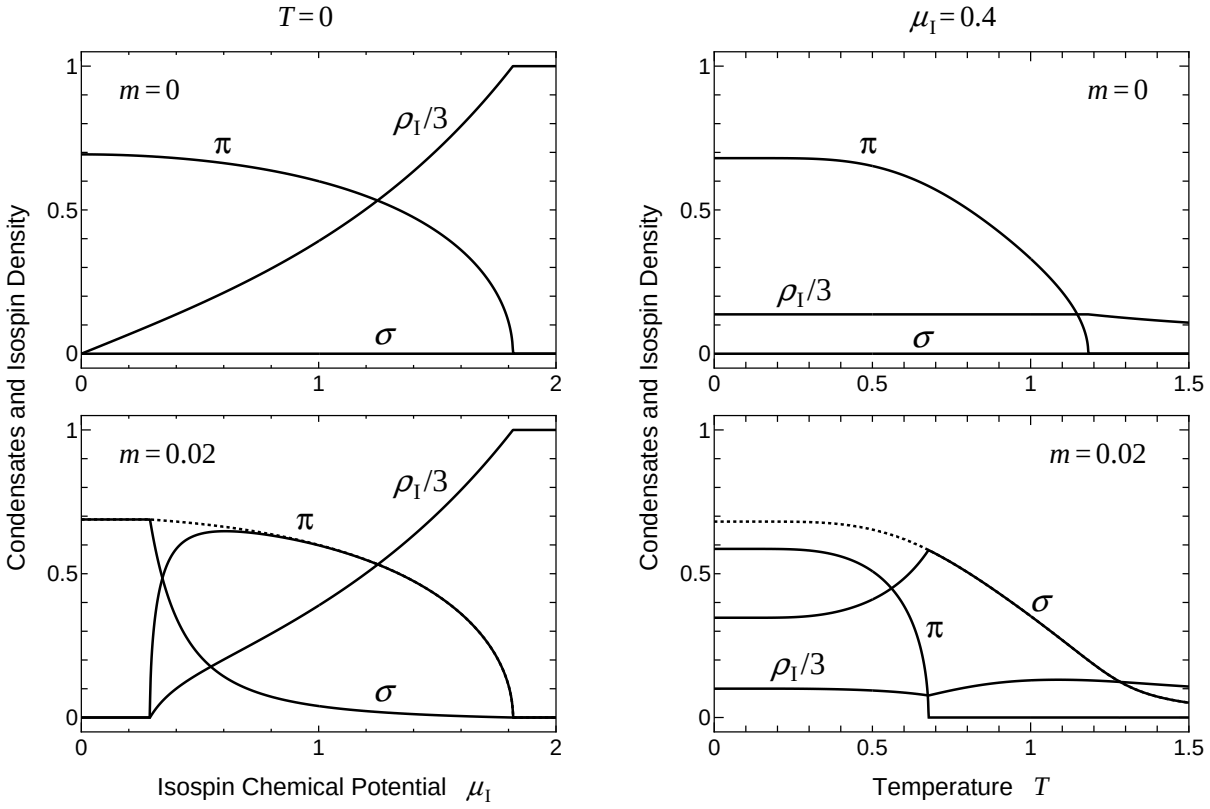

Figure 9: Chiral condensate σ, pion condensate π and isospin density $\rho_{\rm I}$ for $N_{\rm c} = 3, N_{\rm f} = 8$. In the left panels, they are plotted as functions of the isospin chemical potential $\mu_{\rm I}$ at $T = 0$ for $m = 0$ (the upper panel) and $m = 0.02$ (the lower one). In the right panels, they are plotted as functions of the temperature T at $\mu_{\rm I} = 0.4$ for $m = 0$ (the upper panel) and $m = 0.02$ (the lower one). The dotted lines in the lower panels indicate a total magnitude of the condensates $\sqrt{\sigma^2 + \pi^2}$.

This expression can be rewritten as $\mu_{\rm c}^{\rm low} = m_\pi$ with m_π obtained from the excitation spectrum in the vacuum [38] up to the leading order of the $1/d$ expansion. This is nothing but a proof of the fact that the critical value of isospin chemical potential $\mu_{\rm I}^{\rm cri}$ assumed in the previous subsection indeed exists and corresponds to the pion mass.

5.3.1 Condensates, isospin density and phase diagrams

Now we determine the chiral condensate σ and the pion condensate π numerically by minimizing the effective free energy with $N_{\rm f} = 8$ flavors in Eq. (104) for $N_{\rm c} = 3$, $d = 3$. The isospin density $\rho_{\rm I} = -\partial F_{\rm eff}/\partial \mu_{\rm I}$ is also calculated as a function of $\mu_{\rm I}$ and T. We show the results in Fig. 9 for $m = 0$ and $m = 0.02$. The behaviors of σ, π and $\rho_{\rm I}$ are quite similar to those of σ, Δ and $\rho_{\rm B}$ studied for $\mathrm{SU_c}(2)$ QCD, and therefore the discussions in Sec. 3.4 hold true here. Although our results are in principle limited in the strong coupling, the behaviors of σ, π and $\rho_{\rm I}$ as functions of $\mu_{\rm I}$ and T have qualitative agreement with the recent lattice data [16].

And the phase diagram of the strong coupling lattice QCD with $N_{\rm c} = 3, N_{\rm f} = 8$ in the T-$\mu_{\rm I}$ plane and in the three dimensional T-$\mu_{\rm I}$-m space are shown in Fig. 10 and Fig. 11 respectively. The fact that $\mathrm{SU_c}(3)$ QCD at finite isospin density has the same phase structure as that of $\mathrm{SU_c}(2)$ QCD at finite baryon density can be understood from the aspect of the symmetry and its breaking pattern. $\mathrm{SU_c}(3)$ QCD at $\mu_{\rm I} = 0$ and $m = 0$ has chiral symmetry between the chiral condensate and the pion

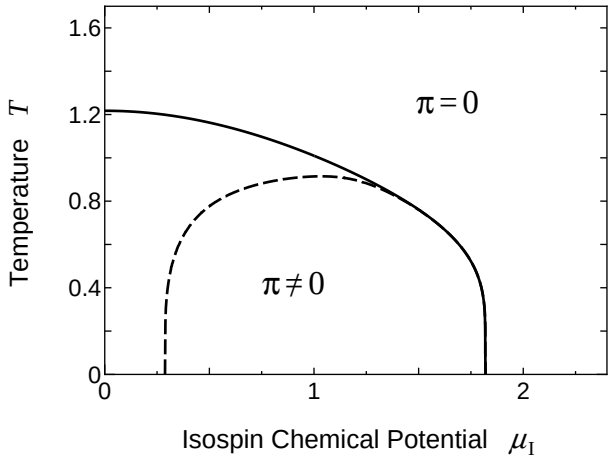

Figure 10: Phase diagram of strong coupling QCD with $N_c = 3, N_f = 8$ in the T-μ_I plane. Solid (dashed) line denotes the critical line for pion condensation for $m = 0$ ($m = 0.02$).

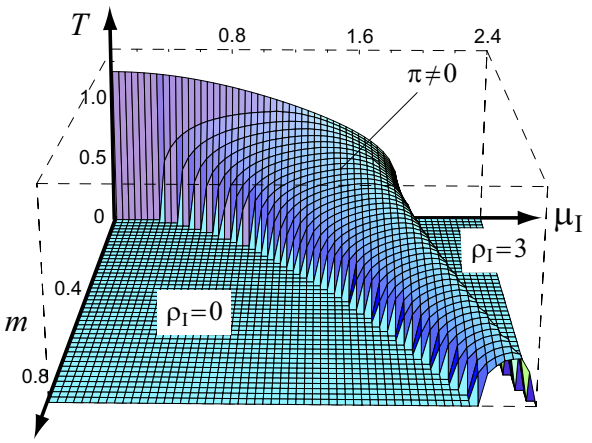

Figure 11: Phase structure of strong coupling QCD with $N_c = 3, N_f = 8$ in the T-μ_I-m space. The surface represents the critical surface for the pion condensation, which separates the region where $\pi \neq 0$ (inside) from the region where $\pi = 0$ (outside).

condensate. On the other hand, $SU_c(2)$ QCD at $\mu_B = 0$ and $m = 0$ has Pauli-Gürsey's symmetry between the chiral condensate and the diquark condensate. In both theories, the introduction of m breaks the symmetries so that the chiral condensate is favored and the introduction of the μ_I/μ_B breaks the symmetries so that the pion/diquark condensate is favored. This is the reason why these two theories have the similar phase structures at finite density.

6 Summary and Discussion

In this thesis, we have studied the phase structure of hot and dense QCD with $N_{\rm c} = 2, 3$ and $N_{\rm f} = 4, 8$ in the strong coupling limit formulated on the lattice. In Sec. 2, we have explained how to derive the effective free energy written in terms of the chiral condensate σ and the diquark condensate Δ at finite temperature T, baryon chemical potential $\mu_{\rm B}$ and quark mass m by employing the $1/d$ expansion (only in the spatial direction).

In Sec. 3, we consider strong coupling lattice QCD with $N_{\rm c} = 2$ (2color-QCD) for $N_{\rm f} = 4$. A major advantage of our approach is that we can derive rather simple formulae in an analytical way for the critical temperature ($T_{\rm c}$), the critical chemical potentials ($\mu_{\rm c}^{\rm low}$ and $\mu_{\rm c}^{\rm up}$) and the baryon density ($\rho_{\rm B}$), which are useful to have physical insight into the problem. Although our results are in principle limited in the strong coupling, the behaviors of σ, Δ and $\rho_{\rm B}$ in the T-$\mu_{\rm B}$-m space have remarkable qualitative agreement with the recent lattice data. Since we do not have to rely on any assumption of small $\mu_{\rm B}$ nor small m in our approach, the strong coupling analysis presented in this thesis is complementary to the results of the chiral perturbation theory and directly provides a useful guide to the lattice 2color-QCD simulations. We have also found that the disappearance of diquark condensation with saturated density can be understood as a Mott-insulating phenomenon.

In Sec. 4, we have investigated the phase structure with $N_{\rm c} = 3$, $N_{\rm f} = 4$ in the T-$\mu_{\rm B}$ plane and the phase transition of chiral restoration was found to be of second order at high temperature region and of first order at low temperature region. Analytical formulae for the critical line of the second order transition and the position of tricritical point were derived. The critical temperature at small quark chemical potential $\mu = \mu_{\rm B}/N_{\rm c}$ can be expanded as $T_{\rm c}(\mu) \simeq T_{\rm c}(0) - 1.5\mu^2/T_{\rm c}(0)$, and the slope was found to be much larger than that calculated in Monte-Carlo lattice simulations [9, 10, 11, 12]. We have discussed that this difference could be understood as the results of the strong coupling limit $g \to \infty$ and the chiral limit $m = 0$. We also studied the effect of finite quark mass on the phase diagram: The position of the critical endpoint has relatively large dependence on the quark mass. Especially for small m, critical endpoint shifts in the direction of smaller T and smaller $\mu_{\rm B}$. This is because the gradient of critical line near the tricritical point is positive, and such a new feature in the phase diagram of QCD should be studied more.

In Sec. 5, we have derived the free energy including isospin chemical potential $\mu_{\rm I}$ and pion condensate π by extending the formulation studied in Sec. 2 with two species of staggered fermion ($N_{\rm f} = 8$) for $N_{\rm c} = 3$. Firstly, we have observed that the critical temperature of chiral restoration decreases by increasing the number of quark flavors due to the thermal excitations of quarks. Then we have studied the effect of small $\mu_{\rm I}$ on the phase diagram in the T-$\mu_{\rm B}$ plane at finite quark mass: Introduction of $\mu_{\rm I}$ splits and shifts the first order phase transition line in the opposite directions of $\mu_{\rm B}$. In addition, $\mu_{\rm I}$ moves two critical endpoints to higher temperatures than that for $\mu_{\rm I} = 0$. This is a non-trivial effect originating from the integration over the temporal gauge link variable at finite temperature which couples up quark sector and down quark one.

Finally we have studied the phase structure in the space of T, $\mu_{\rm I}$ and m and found a formal correspondence between color $\mathrm{SU_c}(3)$ QCD with finite isospin density and color $\mathrm{SU_c}(2)$ QCD with finite baryon density. Such a correspondence can be understood by considering the symmetry and its breaking pattern: chiral (Pauli-Gürsey) symmetry at $m = 0$ and $\mu_{\rm I} = 0$ ($\mu_{\rm B} = 0$) is broken by the quark mass in the direction of chiral condensation, while it is broken by the isospin (baryon) chemical potential in the direction of pion (diquark) condensation. The behaviors of σ, π and $\rho_{\rm I}$ in the T-$\mu_{\rm I}$-m space have again qualitative agreement with the recent lattice data at finite $\mu_{\rm I}$.

There are several directions worth to be explored starting from the present work. Firstly for 2-color QCD, the derivation of an effective action written not only with the chiral and diquark fields but also with the Polyakov loop, $L(\vec{x})$, is interesting because this will allow us a full comparison for all the physical quantities calculated in our formalism and lattice simulations [14]. This is a straightforward generalization of the works in [49], which allows us to analyze $\langle L(\vec{x}) \rangle$ under the influence of chiral and

diquark condensates. Also calculation of the meson and diquark spectra including pseudo-scalar and pseudo-diquark channels will give us deeper understanding about the non-static feature of the present system. Another direction is to study the response of the Bose liquid discussed in this thesis under external fields. Although mesons and diquarks are color neutral in 2-color QCD, they can have electric charge so that the external electromagnetic field leads to a non-trivial change of the phase structure if the field intensity is enough strong.

The remaining work to be explored for $N_{\rm c} \geq 3$ case is to investigate the phase structure with finite $\mu_{\rm B}$ and finite $\mu_{\rm I}$ as well as with T and m, where the non-trivial competition between the chiral and pion condensates takes place. In our formulation, such a study is possible by using the effective free energy given in Eq. (93) with numerical summation over Matsubara frequency and numerical integration over the temporal gauge link variable. How the chiral condensate at finite $\mu_{\rm B}$ is replaced by the pion condensate as increasing $\mu_{\rm I}$ is one of the most interesting problem to be examined.

Acknowledgments

The author is grateful to all members of hadron theory group in University of Tokyo, H. Abuki, K. Fukushima, T. Hatsuda, K. Iida, S. Sasaki and M. Tachibana for discussions on physics. Especially, he thanks to his supervisor Professor Tetsuo Hatsuda for continuous and stimulating discussions on this work and related subjects.

A Summation over the Matsubara frequency

A.1 Case 1

Let us first take the logarithm of Eq.(35);

$$\log\sqrt{\mathrm{Det}[G^{-1}]} = \sum_{n=1}^{N_\tau} \log\left[-\cos^2\left(k_n+\theta/N_\tau\right) + 2Y\cos\left(k_n+\theta/N_\tau\right) + X^2\right] . \tag{110}$$

Here X and Y are defined as

$$X^2 = \cosh^2\mu + M^2 + \left(\frac{d}{2}\right)^2 |\Delta|^2 , \qquad Y = M\sinh\mu . \tag{111}$$

By differentiating $\log\sqrt{\mathrm{Det}[G^{-1}]}$ with respect to X, we obtain

$$\begin{aligned}&\frac{\partial}{\partial X}\log\sqrt{\mathrm{Det}[G^{-1}]} \\ &\quad = \frac{X}{\sqrt{X^2+Y^2}}\sum_{n=1}^{N_\tau}\left[\frac{1}{\cos\left(k_n+\theta/N_\tau\right)-Y+\sqrt{X^2+Y^2}} - \frac{1}{\cos\left(k_n+\theta/N_\tau\right)-Y-\sqrt{X^2+Y^2}}\right] .\end{aligned} \tag{112}$$

Because $\cos(k_n+\theta/N_\tau)$ is invariant under the shift $n\to n+N_\tau$, we can make the summation of n over the range $n=-\infty$ to $n=+\infty$ with an appropriate degeneracy factor Ω. Then the residue theorem enables us to replace the summation by a complex integral as

$$\begin{aligned}\frac{\partial}{\partial X}\log\sqrt{\mathrm{Det}[G^{-1}]} = \frac{X}{\sqrt{X^2+Y^2}}\frac{1}{\Omega}\Bigg[&\oint\frac{\mathrm{d}z}{2\pi\mathrm{i}}\frac{1}{\cos\left(z+\theta/N_\tau\right)+k_-}\frac{-\mathrm{i}N_\tau}{1+\mathrm{e}^{\mathrm{i}N_\tau z}} - \sum_{\bar z}\frac{1}{-\sin\bar z}\frac{-\mathrm{i}N_\tau}{1+\mathrm{e}^{\mathrm{i}N_\tau\bar z}} \\ &- \oint\frac{\mathrm{d}w}{2\pi\mathrm{i}}\frac{1}{\cos\left(w+\theta/N_\tau\right)-k_+}\frac{-\mathrm{i}N_\tau}{1+\mathrm{e}^{\mathrm{i}N_\tau w}} + \sum_{\bar w}\frac{1}{-\sin\bar w}\frac{-\mathrm{i}N_\tau}{1+\mathrm{e}^{\mathrm{i}N_\tau\bar w}}\Bigg] ,\end{aligned} \tag{113}$$

where

$$k_\pm = \sqrt{X^2+Y^2}\pm Y . \tag{114}$$

Owing to the infinite range of the summation over n, we can choose the closed contour at infinity for the complex integrals with respect to z and w, and thus such complex integrals go to zero. $\bar z$ and $\bar w$ are the residues satisfying

$$\cos\left(\bar z+\theta/N_\tau\right)+k_-=0 , \qquad \cos\left(\bar w+\theta/N_\tau\right)-k_+=0 . \tag{115}$$

Solving these equations, we obtain

$$\bar z+\theta/N_\tau = \pm\mathrm{i}E_- +\pi+2\pi n , \qquad \bar w+\theta/N_\tau = \pm\mathrm{i}E_+ +2\pi n , \qquad (n=-\infty,\ldots,\infty) , \tag{116}$$

where

$$E_\pm = \mathrm{arccosh}k_\pm . \tag{117}$$

Substituting Eq. (116) into Eq. (113), we obtain

$$
\begin{aligned}
&\frac{\partial}{\partial X}\log\sqrt{\mathrm{Det}[G^{-1}]} \\
&= \frac{X}{\sqrt{X^2+Y^2}}\frac{1}{\Omega}\sum_{n=-\infty}^{\infty}\left[\frac{1}{-\mathrm{i}\sqrt{k_-^2-1}}\left(\frac{-\mathrm{i}N_\tau}{1+\mathrm{e}^{-N_\tau E_- -\mathrm{i}\theta+\mathrm{i}N_\tau\pi}}-\frac{-\mathrm{i}N_\tau}{1+\mathrm{e}^{N_\tau E_- -\mathrm{i}\theta+\mathrm{i}N_\tau\pi}}\right)\right. \\
&\qquad\left.-\frac{1}{\mathrm{i}\sqrt{k_+^2-1}}\left(\frac{-\mathrm{i}N_\tau}{1+\mathrm{e}^{-N_\tau E_+ -\mathrm{i}\theta}}-\frac{-\mathrm{i}N_\tau}{1+\mathrm{e}^{N_\tau E_+ -\mathrm{i}\theta}}\right)\right] \\
&= \frac{\partial E_-}{\partial X}\left\{\frac{N_\tau}{1+\mathrm{e}^{-N_\tau E_- -\mathrm{i}\theta}}-\frac{N_\tau}{1+\mathrm{e}^{N_\tau E_- -\mathrm{i}\theta}}\right\}+\frac{\partial E_+}{\partial X}\left\{\frac{N_\tau}{1+\mathrm{e}^{-N_\tau E_+ -\mathrm{i}\theta}}-\frac{N_\tau}{1+\mathrm{e}^{N_\tau E_+ -\mathrm{i}\theta}}\right\} \\
&= \frac{\partial}{\partial X}\left[\log\left\{\mathrm{e}^{N_\tau E_-}+\mathrm{e}^{-\mathrm{i}\theta}\right\}+\log\left\{\mathrm{e}^{-N_\tau E_-}+\mathrm{e}^{-\mathrm{i}\theta}\right\}+\log\left\{\mathrm{e}^{N_\tau E_+}+\mathrm{e}^{-\mathrm{i}\theta}\right\}+\log\left\{\mathrm{e}^{-N_\tau E_+}+\mathrm{e}^{-\mathrm{i}\theta}\right\}\right] \\
&= \frac{\partial}{\partial X}\left[-2\mathrm{i}\theta+\log\left\{2\cos\theta+2\cosh N_\tau E_-\right\}+\log\left\{2\cos\theta+2\cosh N_\tau E_+\right\}\right]. \qquad (118)
\end{aligned}
$$

We note that the degeneracy factor Ω is just canceled by the infinite degeneracy of the summation on n. Also we have used the fact that N_τ must be an even integer for the staggered fermion. After the integration with respect to X, we find that $\sqrt{\mathrm{Det}[G^{-1}]}$ is expressed in a rather simple form up to irrelevant factors,

$$
\sqrt{\mathrm{Det}\left[G^{-1}_{ab}(m,n;\theta)\right]} = (2\cos\theta+2\cosh N_\tau E_-)\cdot(2\cos\theta+2\cosh N_\tau E_+)\,. \qquad (119)
$$

This is the final form shown in Eq. (36) in the text.

A.2 Case 2

In this Appendix, we give the formula for the product over the Matsubara frequencies of the expression

$$
I = \prod_{n=1}^{N_\tau/2}\left[\sin^2\bar{k}_n+\lambda^2\right] = \prod_{n=1}^{N_\tau}\left[\sin^2\bar{k}_n+\lambda^2\right]^{\frac{1}{2}} \qquad (120)
$$

with $\bar{k}_n = 2\pi(n-1/2)/N_\tau+\phi/N_\tau-\mathrm{i}\mu$ and N_τ being an even integer. Let us first take the logarithm of above expression and differentiate it with respect to λ;

$$
\frac{\partial}{\partial\lambda}\log I = \sum_{n=1}^{N_\tau}\frac{\lambda}{\sin^2\bar{k}_n+\lambda^2}\,. \qquad (121)
$$

Because $\sin(k_n+\phi/N_\tau-\mathrm{i}\mu)$ is invariant under the shift $n\to n+N_\tau$, we can make the summation of n over the range $n=-\infty$ to $n=+\infty$ with an appropriate degeneracy factor Ω. Then the residue theorem enables us to replace the summation by a complex integral as

$$
\begin{aligned}
\frac{\partial}{\partial\lambda}\log I = \frac{1}{\Omega}\left[\oint\frac{\mathrm{d}z}{2\pi\mathrm{i}}\frac{\lambda}{\sin^2(z+\phi/N_\tau-\mathrm{i}\mu)+\lambda^2}\frac{-\mathrm{i}N_\tau}{1+\mathrm{e}^{\mathrm{i}N_\tau z}}\right. \\
\left.-\sum_{\bar{z}}\frac{\lambda}{2\sin(\bar{z}+\phi/N_\tau-\mathrm{i}\mu)\cos(\bar{z}+\phi/N_\tau-\mathrm{i}\mu)}\frac{-\mathrm{i}N_\tau}{1+\mathrm{e}^{\mathrm{i}N_\tau\bar{z}}}\right]. \qquad (122)
\end{aligned}
$$

Owing to the infinite range of the summation over n, we can choose the closed contour at infinity for the complex integrals with respect to z, and thus such complex integrals go to zero. $\bar{z}$ are the residues satisfying

$$
\sin^2(\bar{z}+\phi/N_\tau-\mathrm{i}\mu)+\lambda^2 = 0\,. \qquad (123)
$$

Solving this equation, we obtain

$$\bar{z} + \phi/N_\tau - \mathrm{i}\mu = \pm \mathrm{i}E + 2\pi n\,, \quad \pm \mathrm{i}E + \pi + 2\pi n\,, \tag{124}$$

with $E = \mathrm{arcsinh}\lambda$ and $n = -\infty, \ldots, \infty$. Substituting Eq. (124) into Eq. (122), we obtain

$$\begin{aligned}
\frac{\partial}{\partial\lambda}\log I &= \frac{1}{\Omega}\sum_{n=-\infty}^{\infty}\frac{1}{\cosh E}\left[\frac{N_\tau}{1+\mathrm{e}^{-N_\tau E - \mathrm{i}\phi - N_\tau\mu}} - \frac{N_\tau}{1+\mathrm{e}^{N_\tau E - \mathrm{i}\phi - N_\tau\mu}}\right] \\
&= \frac{\partial E}{\partial\lambda}\left[\frac{N_\tau}{1+\mathrm{e}^{-N_\tau E - \mathrm{i}\phi - N_\tau\mu}} - \frac{N_\tau}{1+\mathrm{e}^{N_\tau E - \mathrm{i}\phi - N_\tau\mu}}\right] \\
&= \frac{\partial}{\partial\lambda}\left[\log\left\{\mathrm{e}^{N_\tau E} + \mathrm{e}^{-\mathrm{i}\phi - N_\tau\mu}\right\} + \log\left\{\mathrm{e}^{-N_\tau E} + \mathrm{e}^{-\mathrm{i}\phi - N_\tau\mu}\right\}\right] \\
&= \frac{\partial}{\partial\lambda}\left[-\mathrm{i}\phi - N_\tau\mu + \log\left\{2\cosh\left[N_\tau E\right] + 2\cos[\phi - \mathrm{i}N_\tau\mu]\right\}\right]\,.
\end{aligned} \tag{125}$$

We note that the degeneracy factor Ω is just cancelled by the infinite degeneracy of the summation on n. After the integration with respect to λ, we find that the result is expressed in a rather simple form up to irrelevant factors,

$$I = 2\cosh\left[N_\tau E\right] + 2\cos[\phi - \mathrm{i}N_\tau\mu] \tag{126}$$

with $E = \mathrm{arcsinh}\lambda$.

B Proof of $\sigma = 0$ at the global minimum of $F_{\mathrm{eff}}[\sigma, \Delta]|_{m=0}$

For $m = 0$, it is useful to rewrite the free energy Eq. (40) in terms of the radial and angle variables,

$$\sigma = \lambda\sin\phi\,, \qquad |\Delta| = \lambda\cos\phi\,. \tag{127}$$

Then the free energy is

$$F_{\mathrm{eff}}[\lambda,\phi] = \frac{d}{2}\lambda^2 - T\log\left\{1 + 4\cosh\left(E_+/T\right)\cdot\cosh\left(E_-/T\right)\right\}\,, \tag{128}$$

with the quasi-quark energy given by

$$E_\pm = \mathrm{arccosh}\left(\sqrt{(d/2)^2\lambda^2 + \cosh^2\mu + (d/2)^2\lambda^2\sinh^2\mu\sin^2\phi} \pm \frac{d}{2}\lambda\sinh\mu\sin\phi\right)\,. \tag{129}$$

What we are going to prove here is that $F_{\mathrm{eff}}[\lambda,\phi]$ has the global minimum at $\phi = 0$ for arbitrary T, μ, and λ. Actually we can prove the following statement in a more abstract expression;

> $\cosh\{a\,\mathrm{arccosh}(b\,\mathrm{e}^{c})\}\cdot\cosh\{a\,\mathrm{arccosh}(b\,\mathrm{e}^{-c})\}$ has the global maximum at $c = 0\,$,
> where $a > 1,\ b > 1,$ and $-\log b < c < \log b\,$.

We can apply this corollary to our problem to prove that $\phi = 0$ is the global minimum of the free energy. Obviously $\phi = 0$ turns out to be the global maximum of $\cosh(E_+/T)\cdot\cosh(E_-/T)$ once we substitute,

$$a = 1/T, \quad b = \sqrt{(d/2)^2\lambda^2 + \cosh^2\mu}, \quad c = \log\left[\sqrt{1 + (d\lambda/2b)^2\sinh^2\mu\sin^2\phi} + (d\lambda/2b)\sinh\mu\sin\phi\right]\,. \tag{130}$$

Thus we have proven that $F_{\mathrm{eff}}[\lambda,\phi]$ is globally minimized at $\phi = 0$, in other words, the chiral condensate vanishes in the chiral limit.

C SU(N_c) integration in the Polyakov gauge

In this Appendix, we give the formula for the SU(N_c) integration

$$J = \int \mathrm{d}U_0 \, F(U_0) \, . \tag{131}$$

Here we consider the function which can be written by the product of $f(\theta_a)$ in the Polyakov gauge as

$$F(U_0) = \prod_{a=1}^{N_c} f\left(\theta_a\right) \, . \tag{132}$$

Since the SU(N_c) Haar measure in the Polyakov gauge is given by

$$\begin{aligned} \int \mathrm{d}U_0 &= \int_{-\pi}^{\pi} \prod_{a=1}^{N_c} \frac{\mathrm{d}\phi_a}{2\pi} \prod_{a<b} \left| \mathrm{e}^{\mathrm{i}\phi_a} - \mathrm{e}^{\mathrm{i}\phi_b} \right|^2 \Big|_{\sum_a \phi_a = 0} \\ &= \int_{-\pi}^{\pi} \prod_{a=1}^{N_c} \frac{\mathrm{d}\phi_a}{2\pi} \left| \epsilon_{i_1 \cdots i_{N_c}} \mathrm{e}^{\mathrm{i}\phi_1 (N_c - i_1)} \cdots \mathrm{e}^{\mathrm{i}\phi_{N_c} (N_c - i_{N_c})} \right|^2 \cdot 2\pi \, \delta\left(\sum \phi_a \right) \, , \end{aligned} \tag{133}$$

the integration becomes

$$J = \int_{-\pi}^{\pi} \prod_{a=1}^{N_c} \frac{\mathrm{d}\phi_a}{2\pi} \left| \epsilon_{i_1 \cdots i_{N_c}} \mathrm{e}^{\mathrm{i}\phi_1 (N_c - i_1)} \cdots \mathrm{e}^{\mathrm{i}\phi_{N_c} (N_c - i_{N_c})} \right|^2 \cdot 2\pi \, \delta\left(\sum_{a=1}^{N_c} \phi_a \right) \times \prod_{a=1}^{N_c} f\left(\theta_a\right) \, . \tag{134}$$

Because the delta function can be rewritten as

$$2\pi \, \delta\left(\sum_{a=1}^{N_c} \phi_a \right) = \sum_{n=-\infty}^{\infty} \exp\left[-\mathrm{i}n \sum_{a=1}^{N_c} \phi_a \right] \, , \tag{135}$$

we obtain

$$J = \sum_{n=-\infty}^{\infty} \epsilon_{i_1 \cdots i_{N_c}} \epsilon_{j_1 \cdots j_{N_c}} \prod_{a=1}^{N_c} \int_{-\pi}^{\pi} \frac{\mathrm{d}\phi_a}{2\pi} f(\phi_a) \exp\left[-\mathrm{i} \left(n + i_a - j_a \right) \phi_a \right] = N_c! \sum_{n=-\infty}^{\infty} \det_{i,j} M_{n+i-j} \, . \tag{136}$$

Here we have defined M_n as

$$M_n = \int_{-\pi}^{\pi} \frac{\mathrm{d}\phi}{2\pi} f(\phi) \exp\left[-\mathrm{i}n\phi \right] \, , \tag{137}$$

and the determinant is to be taken with respect to $i, j = 1, 2, \cdots, N_c$.

References

[1] The latest results of the PHOBOS, PHENIX, STAR and BRAHMS collaborations at RHIC are in B. B. Back *et al.*, Phys. Rev. Lett. **91**, 072302 (2003);
S. S. Adler *et al.*, Phys. Rev. Lett. **91**, 072303 (2003);
J. Adams *et al.*, Phys. Rev. Lett. **91**, 072304 (2003);
I. Arsene *et al.*, Phys. Rev. Lett. **91**, 072305 (2003).

[2] For a recent review on the signal of the quark gluon plasma, see
M. Gyulassy, I. Vitev, X.-N. Wang, B.-W. Zhang, nucl-th/0302077.

[3] R. Tamagaki, Prog. Theor. Phys. **44**, 905 (1970).
M. Hoffberg, A. E. Glassgold, R. W. Richardson and M. Ruderman, Phys. Rev. Lett. **24**, 775 (1970).
For further references, see the review: T. Kunihiro, T. Muto, T. Takatsuka, R. Tamagaki and T. Tatsumi, Prog. Theor. Phys. Suppl. **112**, 1 (1993).

[4] A. B. Migdal, Nucl. Phys. **A210**, 421 (1972).
R. F. Sawyer and D.J. Scalapino, Phys. Rev. D **7**, 953 (1973).
For further references, see the review in [3].

[5] D. B. Kaplan and A. E. Nelson, Phys. Lett. B **175**, 57 (1986).
For further references, see the review: C. H. Lee, Phys. Rep. **275**, 255 (1996).

[6] The possibility of superconducting quark matter was originally studied in B. C. Barrois, Nucl. Phys. **B129**, 390 (1977); D. Bailin and A. Love, Phys. Rep. **107**, 325 (1984).
For the recent progress on such a system, see K. Rajagopal and F. Wilczek, in *At the Frontier of Particle Physics: Handbook of QCD*, edited by M. Shifman (World Scientific, Singapore, 2001), p. 2061, hep-ph/0011333; M. G. Alford, Ann. Rev. Nucl. Part. Sci. **51**, 131 (2001).

[7] See, for example, F. Karsch, Lect. Notes Phys. **583**, 209 (2002).
S. D. Katz, hep-lat/0310051.

[8] For an introductory review on the lattice QCD at finite density and related works, see S. Muroya, A. Nakamura, C. Nonaka and T. Takaishi, Prog. Theor. Phys. **110**, 615 (2003).

[9] Z. Fodor and S.D. Katz, Phys. Lett. B **534**, 87 (2002); J. High Energy Phys. **03**, 014 (2002).

[10] C.R. Allton, S. Ejiri, S. J. Hands, O. Kaczmarek, F. Karsch, E. Laermann, Ch. Schmidt and L. Scorzato, Phys. Rev. D **66**, 074507 (2002).

[11] P. de Forcrand and O. Philipsen, Nucl. Phys. **B642**, 290 (2002); Nucl. Phys. **B673**, 170 (2003).

[12] M. D'Elia and M.-P. Lombardo, Phys. Rev. D **67**, 014505 (2003).

[13] S. Hands, J. B. Kogut, M.-P. Lombardo and S. E. Morrison, Nucl. Phys. **B558**, 327 (1999).
S. Hands, I. Montvay, S. Morrison, M. Oevers, L. Scorzato and J. Skullerud, Eur. Phys. J. C **17**, 285 (2000).

[14] J.B. Kogut, D. Toublan and D.K. Sinclair, Phys. Lett. B **514**, 77 (2001); Nucl. Phys. **B642**, 181 (2002); Phys. Rev. D **68**, 054507 (2003).
J. B. Kogut, D. K. Sinclair, S. J. Hands and S. E. Morrison, Phys. Rev. D **64**, 094505 (2001).

[15] D. T. Son and M. A. Stephanov, Phys. Rev. Lett. **86**, 592 (2001); Phys. At. Nucl. **64**, 899 (2001).
T. D. Cohen, Phys. Rev. Lett. **91**, 032002 (2003); Phys. Rev. Lett. **91**, 222001 (2003).

[16] J.B. Kogut and D.K. Sinclair, Phys. Rev. D **66**, 014508 (2002); Phys. Rev. D **66**, 034505 (2002).

[17] E. Dagotto, F. Karsch and A. Moreo, Phys. Lett. B **169**, 421 (1986).

[18] E. Dagotto, A. Moreo and U. Wolff, Phys. Lett. B **186**, 395 (1987).

[19] J. U. Klatke and K. H. Mutter, Nucl. Phys. **B342**, 764 (1990).

[20] P. H. Damgaard, N. Kawamoto and K. Shigemoto, Phys. Rev. Lett. **53**, 2211 (1984); Nucl. Phys. **B264**, 1 (1986)
P. H. Damgaard, D. Hochberg and N. Kawamoto, Phys. Lett. B **158**, 239 (1985).

[21] E.-M. Ilgenfritz and J. Kripfganz, Z. Phys. C **29**, 79 (1985).
G. Fäldt and B. Petersson, Nucl. Phys. **B264** [FS15], 197 (1986).
N. Bilić, K. Demeterfi and B. Petersson, Nucl. Phys. **B377**, 651 (1992).
N. Bilić, F. Karsch and K. Redlich, Phys. Rev. D **45**, 3228 (1992).

[22] N. Bilić and J. Cleymans, Phys. Lett. B **335**, 266 (1995).

[23] R. Aloisio, V. Azcoiti, G. Di Carlo, A. Galante and A. F. Grillo, Nucl. Phys. **B564**, 489 (2000).
E. B. Gregory, S.-H Guo, H. Kröger and X.-Q. Luo, Phys. Rev. D **62**, 054508 (2000).

[24] Y. Umino, Phys. Rev. D **66**, 074501 (2002).
B. Bringoltz and B. Svetitsky, Phys. Rev. D **68**, 034501 (2003).
V. Azcoiti, G. Di Carlo, A. Galante and V. Laliena, J. High Energy Phys. **0309**, 014 (2003).
S. Chandrasekharan and F.-J. Jiang, Phys. Rev. D **68**, 091501 (2003).

[25] K. Fukushima, hep-ph/0312057.

[26] M. Asakawa and K. Yazaki, Nucl. Phys. **A504**, 668 (1989).
J. Berges and K. Rajagopal, Nucl. Phys. **B538**, 215 (1999).

[27] M. A. Stephanov, Phys. Rev. Lett. **76**, 4472 (1996).
M. A. Halasz, A. D. Jackson, R. E. Shrock, M. A. Stephanov and J. J. M. Verbaarschot, Phys. Rev. D **58**, 096007 (1998).

[28] C. D. Roberts and S. M. Schmidt, Prog. Part. Nucl. Phys. **45**, S1 (2000), and references therein.
T. Ikeda, Prog. Theor. Phys. **107**, 403 (2002).
S. Takagi, Prog. Theor. Phys. **109**, 233 (2003).

[29] A. Barducci, R. Casalbuoni, S. De Curtis, R. Gatto and G. Pettini, Phys. Rev. D **41**, 1610 (1990).
A. Barducci, R. Casalbuoni, G. Pettini and R. Gatto, Phys. Rev. D **49**, 426 (1994).

[30] Y. Nishida, K. Fukushima and T. Hatsuda, hep-ph/0306066 to appear in Phys. Rep. (2004).
Y. Nishida, hep-ph/0310160 to appear in Prog. Theor. Phys. Suppl. (2004).

[31] Y. Nishida, hep-ph/0312371.

[32] J. B. Kogut and L. Susskind, Phys. Rev. D **11**, 395 (1975).
T. Banks, J. B. Kogut and L. Susskind, Phys. Rev. D **13**, 1043 (1976).
L. Susskind, Phys. Rev. D **16**, 3031 (1977).
See also textbooks on lattice gauge theory, e.g., I. Montray and G. Münster, *Quantum Fields on a Lattice* (Cambridge University Press, Cambridge, 1994).

[33] W. Pauli, Nuovo Cimento **6**, 205 (1957).
F. Gürsey, Nuovo Cimento **7**, 411 (1958).

[34] H. Abuki, T. Hatsuda and K. Itakura, Phys. Rev. D **65**, 074014 (2002).
K. Itakura, Nucl. Phys. **A715**, 859 (2003).

[35] This integral is known as the pfaffian. See e.g., J. Zinn-Justin, *Quantum Field Theory and Critical Phenomena* (Clarendon Press, Oxford, 1989), Chapter 1.

[36] J.B. Kogut, M.A. Stephanov and D. Toublan, Phys. Lett. B **464**, 183 (1999).
J.B. Kogut, M.A. Stephanov, D. Toublan, J.J.M. Verbaarschot, and A. Zhitnitsky, Nucl. Phys. **B582**, 477 (2000).

[37] K. Splittorff, D. Toublan and J.J.M. Verbaarschot, Nucl. Phys. **B639**, 524 (2002).

[38] H. Kluberg-Stern, A. Morel and B. Petersson, Nucl. Phys. **B215** [FS7], 527 (1983).
H. Kluberg-Stern, A. Morel, O. Napoly and B. Petersson, Nucl. Phys. **B220** [FS8], 447 (1983).
T. Jolicoeur, H. Kluberg-Stern, A. Morel, M. Lev and B. Petersson, Nucl. Phys. **B235** [FS11], 455 (1984).

[39] N. Kawamoto and J. Smit, Nucl. Phys. **B192**, 100 (1981).

[40] C. Van den Doel and J. Smit, Nucl. Phys. **B228**, 122 (1983).
M. F. L. Golterman and J. Smit, Nucl. Phys. **B245**, 61 (1984).

[41] N. G. Antoniou and A. S. Kapoyannis, Phys. Lett. B **563**, 165 (2003).

[42] Y. Hatta and T. Ikeda, Phys. Rev. D **67**, 014028 (2003).

[43] F. Karsch, C. R. Allton, S. Ejiri, S. J. Hands, O. Kaczmarek, E. Laermann and C. Schmidt, hep-lat/0309116.

[44] B. Klein, D. Toublan and J. J. M. Verbaarschot, Phys. Rev. D **68**, 014009 (2003).

[45] M. Frank, M. Buballa and M. Oertel, Phys. Lett. B **562**, 221 (2003).
D. Toublan and J. B. Kogut, Phys. Lett. B **564**, 212 (2003).

[46] A. Barducci, G. Pettini, L. Ravagli and R. Casalbuoni, Phys. Lett. B **564**, 217 (2003).

[47] B. Vanderheyden and A. D. Jackson, Phys. Rev. D **64**, 074016 (2001).

[48] G. Schmid, S. Todo, M. Troyer and A. Dorneich, cond-mat/0110024.

[49] K. Fukushima, Phys. Lett. B **553**, 38 (2003); Phys. Rev. D **68**, 045004 (2003).